

Alma Mater Studiorum Università di Bologna  
Archivio istituzionale della ricerca

Reactions of  $[\text{Pt}_6(\text{CO})_6(\text{SnX}_2)_2(\text{SnX}_3)_4]^{4-}$  ( $\text{X} = \text{Cl}, \text{Br}$ ) with Acids: Syntheses and molecular structures of  $[\text{Pt}_{12}(\text{CO})_{10}(\text{SnCl})_2(\text{SnCl}_2)_4\text{Cl}_2\text{Sn}(\mu\text{-OH})\text{SnCl}_2]^{2-}$  And  $[\text{Pt}_7(\text{CO})_6(\text{SnBr}_2)_4\text{Br}_2\text{Sn}(\mu\text{-OH})\text{SnBr}_2\text{Br}_2\text{Sn}(\mu\text{-Br})\text{SnBr}_2]^{2-}$  Platinum carbonyl clusters decorated by Sn(II)-Fragments

This is the final peer-reviewed author's accepted manuscript (postprint) of the following publication:

*Published Version:*

Berti, B., Bortoluzzi, M., Cesari, C., Femoni, C., Iapalucci, M.C., Zacchini, S. (2020). Reactions of  $[\text{Pt}_6(\text{CO})_6(\text{SnX}_2)_2(\text{SnX}_3)_4]^{4-}$  ( $\text{X} = \text{Cl}, \text{Br}$ ) with Acids: Syntheses and molecular structures of  $[\text{Pt}_{12}(\text{CO})_{10}(\text{SnCl})_2(\text{SnCl}_2)_4\text{Cl}_2\text{Sn}(\mu\text{-OH})\text{SnCl}_2]^{2-}$  And  $[\text{Pt}_7(\text{CO})_6(\text{SnBr}_2)_4\text{Br}_2\text{Sn}(\mu\text{-OH})\text{SnBr}_2\text{Br}_2\text{Sn}(\mu\text{-Br})\text{SnBr}_2]^{2-}$  Platinum carbonyl clusters decorated by Sn(II)-Fragments. *INORGANICA CHIMICA ACTA*, 503, 119432-119432 [10.1016/j.ica.2020.119432].

*Availability:*

This version is available at: <https://hdl.handle.net/11585/725477> since: 2020-02-28

*Published:*

DOI: <http://doi.org/10.1016/j.ica.2020.119432>

*Terms of use:*

Some rights reserved. The terms and conditions for the reuse of this version of the manuscript are specified in the publishing policy. For all terms of use and more information see the publisher's website.

This is the final peer-reviewed accepted manuscript of:

B. Berti, M. Bortoluzzi, C. Cesari, C. Femoni, M. C. Iapalucci, S. Zacchini, "Reactions of  $[\text{Pt}_6(\text{CO})_6(\text{SnX}_2)_2(\text{SnX}_3)_4]^{4-}$  (X = Cl, Br) with Acids: Syntheses and molecular structures of  $[\text{Pt}_{12}(\text{CO})_{10}(\text{SnCl})_2(\text{SnCl}_2)_4\{\text{Cl}_2\text{Sn}(\mu\text{-OH})\text{SnCl}_2\}_2]^{2-}$  And  $[\text{Pt}_7(\text{CO})_6(\text{SnBr}_2)_4\{\text{Br}_2\text{Sn}(\mu\text{-OH})\text{SnBr}_2\}\{\text{Br}_2\text{Sn}(\mu\text{-Br})\text{SnBr}_2\}]^{2-}$  Platinum carbonyl clusters decorated by Sn(II)-Fragments", *Inorg. Chim. Acta* **2020**, 503, 119432.

The final published version is available online at:  
<https://doi.org/10.1016/j.ica.2020.119432>

Rights / License: Licenza per Accesso Aperto. Creative Commons Attribuzione - Non commerciale - Non opere derivate 4.0 (CCBYNCND)

The terms and conditions for the reuse of this version of the manuscript are specified in the publishing policy. For all terms of use and more information see the publisher's website.

This item was downloaded from IRIS Università di Bologna (<https://cris.unibo.it/>)

**When citing, please refer to the published version.**

# Reactions of $[\text{Pt}_6(\text{CO})_6(\text{SnX}_2)_2(\text{SnX}_3)_4]^{4-}$ ( $\text{X} = \text{Cl}, \text{Br}$ ) with Acids: Syntheses and Molecular Structures of $[\text{Pt}_{12}(\text{CO})_{10}(\text{SnCl})_2(\text{SnCl}_2)_4\{\text{Cl}_2\text{Sn}(\mu\text{-OH})\text{SnCl}_2\}_2]^{2-}$ and $[\text{Pt}_7(\text{CO})_6(\text{SnBr}_2)_4\{\text{Br}_2\text{Sn}(\mu\text{-OH})\text{SnBr}_2\}\{\text{Br}_2\text{Sn}(\mu\text{-Br})\text{SnBr}_2\}]^{2-}$ Platinum Carbonyl Clusters Decorated by Sn(II)-Fragments

Beatrice Berti,<sup>a</sup> Marco Bortoluzzi,<sup>b</sup> Cristiana Cesari,<sup>a</sup> Cristina Femoni,<sup>a</sup> Maria Carmela Iapalucci,<sup>a</sup>  
and Stefano Zacchini<sup>\*,a</sup>

<sup>a</sup> Dipartimento di Chimica Industriale "Toso Montanari", University of Bologna, Viale Risorgimento 4, I-40136 Bologna Italy. E-mail: stefano.zacchini@unibo.it; Web: <https://www.unibo.it/sitoweb/stefano.zacchini/en>; Tel: +39 051 2093711.

<sup>b</sup> Dipartimento di Scienze Molecolari e Nanosistemi, Ca' Foscari University of Venice, Via Torino 155 – 30175 Mestre (Ve), Italy.

**Abstract:** The reactions of  $[\text{Pt}_6(\text{CO})_6(\text{SnX}_2)_2(\text{SnX}_3)_4]^{4-}$  ( $\text{X} = \text{Cl}$ , **1**;  $\text{Br}$ , **2**) with an excess of  $\text{HBF}_4 \cdot \text{Et}_2\text{O}$  afforded the new  $[\text{Pt}_{12}(\text{CO})_{10}(\text{SnCl})_2(\text{SnCl}_2)_4\{\text{Cl}_2\text{Sn}(\mu\text{-OH})\text{SnCl}_2\}_2]^{2-}$  (**3**) and  $[\text{Pt}_7(\text{CO})_6(\text{SnBr}_2)_4\{\text{Br}_2\text{Sn}(\mu\text{-OH})\text{SnBr}_2\}\{\text{Br}_2\text{Sn}(\mu\text{-Br})\text{SnBr}_2\}]^{2-}$  (**4**) heterometallic clusters. The molecular structures of **3** and **4** were determined by means of single crystal X-ray diffraction. The bonding within these bimetallic Pt-Sn clusters were investigated computationally by means of DFT methods and Atoms-In-Molecules analyses. **3** and **4** displayed a low valent Pt core stabilised by the interaction with CO and Sn(II) based ligands. The solid state structures of these clusters revealed the presence on H-bonds involving the OH-groups of the  $\{\text{X}_2\text{Sn}(\mu\text{-OH})\text{SnX}_2\}^-$  ligands.

**Keywords:** Cluster compounds; Carbonyl ligands; Platinum; Tin; Structure elucidation

## 1. Introduction

Several bimetallic Pt-Sn carbonyl clusters whose structures have been determined by means of single-crystal X-ray diffraction have been reported to date, that is  $[\text{Pt}_8(\text{CO})_{10}(\text{SnCl}_2)_4]^{2-}$  [**1**],  $[\text{Pt}_5(\text{CO})_5\{\text{Cl}_2\text{Sn}(\text{OR})\text{SnCl}_2\}_3]^{3-}$  ( $\text{R} = \text{H}, \text{Me}, \text{Et}, ^i\text{Pr}$ ) [**2**],  $[\text{Pt}_6(\text{CO})_6(\text{SnCl}_2)_2(\text{SnCl}_3)_4]^{4-}$  [**3**],  $[\text{Pt}_9(\text{CO})_8(\text{SnCl}_2)_3(\text{SnCl}_3)_2(\text{Cl}_2\text{SnOCOSnCl}_2)]^{4-}$  [**3**],  $[\text{Pt}_{10}(\text{CO})_{14}\{\text{Cl}_2\text{Sn}(\text{OH})\text{SnCl}_2\}_2]^{2-}$  [**3**],  $[\text{Pt}_6(\text{CO})_8(\text{SnCl}_2)(\text{SnCl}_3)_4]^{4-}$

*This item was downloaded from IRIS Università di Bologna (<https://cris.unibo.it/>)*

**When citing, please refer to the published version.**

[4], and  $[\text{Pt}_6(\text{CO})_8(\text{SnCl}_2)(\text{SnCl}_3)_2(\text{PPh}_3)_2]^{2-}$  [4]. These clusters were composed of a low valent Pt-CO core decorated on the surface by miscellaneous Sn(II) fragments. These included  $\text{SnCl}_2$ ,  $[\text{SnCl}_3]^-$ ,  $[\text{Cl}_2\text{Sn}(\text{OR})\text{SnCl}_2]^-$ , and  $[\text{Cl}_2\text{SnOCOSnCl}_2]^{2-}$ . In this sense,  $[\text{SnCl}_3]^-$  ligands have been employed also for the stabilisation of ultra-small Pt nanoparticles [5].

The Pt-Sn bonds within these clusters may be described as Lewis type acid-base interactions, where each Sn atom acted as a two-electron donor. Thus, the common feature to all of these clusters was the perfect segregation of the two metals. This was due to the fact that platinum was a noble metal which formed strong Pt-Pt bonds and preferred to adopt a low (close to zero) oxidation state. Conversely, tin was more electropositive and showed high affinity for halides and oxygen. Thus, it preferred to adopt a positive oxidation state and formed strong Sn-X (X = halogen) and Sn-O interactions [6]. At the same time, Pt-Sn bonds were rather strong and, therefore, Sn-fragments were very effective as surface ligands for the stabilisation of low valent Pt clusters, nanoclusters and nanoparticles. Indeed, several complexes containing direct Pt-Sn bonds have reported and the nature of the Pt-Sn covalent bond studied in detail [7,8].

This behaviour might be related to the fact that tin was often employed as modifier and promoter of Pt-based homogeneous and heterogeneous catalysts. Reactions for which Pt-Sn synergy was beneficial included hydrogenation, hydroformylation, water-gas shift reaction, dehydrogenation and petroleum reforming [9-15]. More recently, Pt-Sn nanoparticles were employed also for applications in electrocatalysis [16-19]. We demonstrated that molecular Pt-Sn carbonyl clusters were well suited precursors for the synthesis of supported metal catalysts for the selective oxidation of 5-hydroxymethylfurfural (HMF) [20]. In particular, the synthesis of  $\text{TiO}_2$ -supported Pt-Sn nanoparticles from molecular carbonyl cluster decomposition showed the crucial role played by the synthetic strategy on the preparation of active and stable Pt-based supported catalysts. Moreover, the addition of Sn to Pt was demonstrated to lead to the formation of unique active sites with significant improved stability in the base-free oxidation of HMF.

In order to widen the scope of our study and deepen our understanding of the Pt-Sn interactions occurring on molecular polyatomic aggregates, we investigated the reactivity of the  $[\text{Pt}_6(\text{CO})_6(\text{SnCl}_2)_2(\text{SnCl}_3)_4]^{4-}$  (**1**) bimetallic cluster and its Br-congener  $[\text{Pt}_6(\text{CO})_6(\text{SnBr}_2)_2(\text{SnBr}_3)_4]^{4-}$  (**2**) towards strong acids. Indeed, it was reported in the literature that strong acids may induce the rearrangement and growth of metal carbonyl clusters [21,22]. Thus, the aim of the present work was to obtain larger Pt-Sn clusters. Interestingly, the outcome of these reactions strongly depended on the halogen present, resulting in the formation of  $[\text{Pt}_{12}(\text{CO})_{10}(\text{SnCl})_2(\text{SnCl}_2)_4\{\text{Cl}_2\text{Sn}(\mu\text{-OH})\text{SnCl}_2\}_2]^{2-}$  (**3**) when X = Cl and  $[\text{Pt}_7(\text{CO})_6(\text{SnBr}_2)_4\{\text{Br}_2\text{Sn}(\mu\text{-OH})\text{SnBr}_2\}\{\text{Br}_2\text{Sn}(\mu\text{-Br})\text{SnBr}_2\}]^{2-}$  (**4**) when X = Br. The solid state structures of these clusters revealed the presence of H-bonds involving the OH-groups of the  $\{\text{X}_2\text{Sn}(\text{OH})\text{SnX}_2\}^-$  ligands. The

*This item was downloaded from IRIS Università di Bologna (<https://cris.unibo.it/>)*

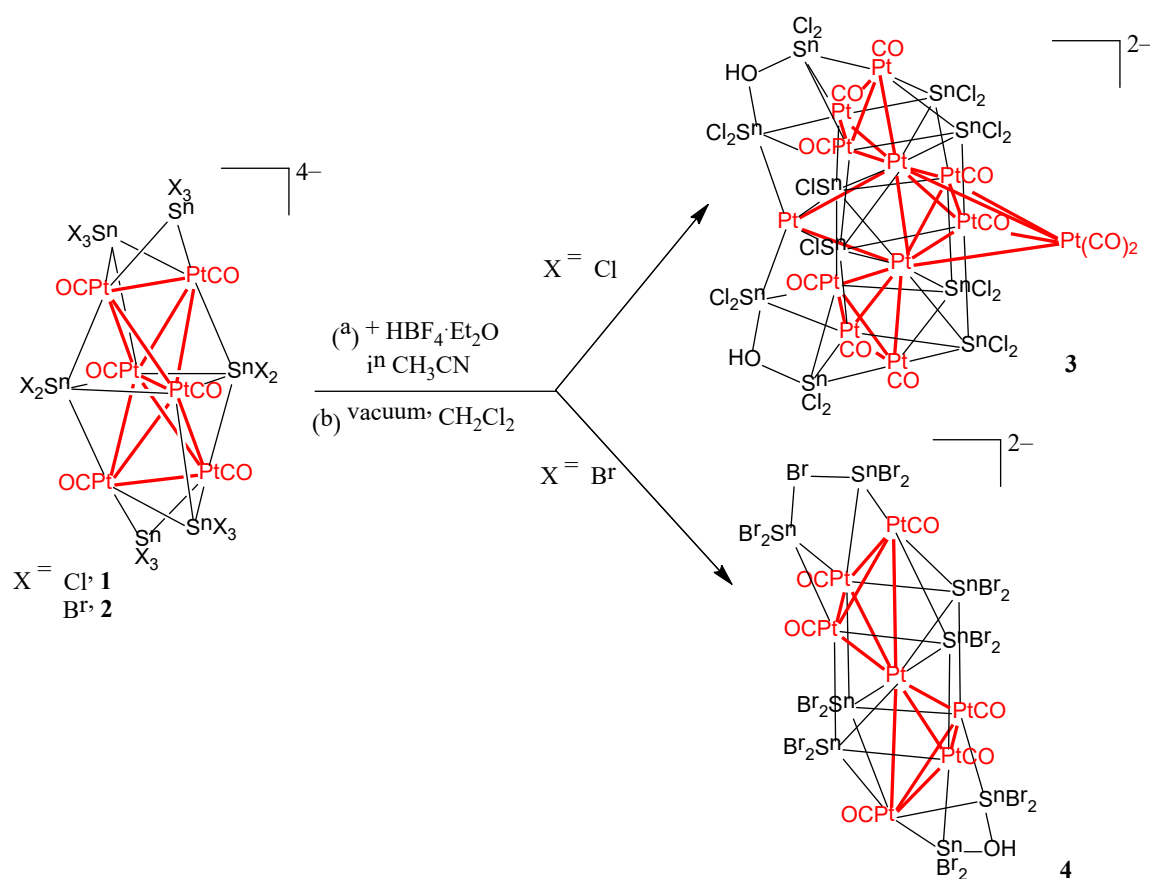
***When citing, please refer to the published version.***

bonding within these bimetallic Pt-Sn clusters were investigated computationally by means of DFT methods and Atoms-In-Molecules analyses.

## 2. Results and Discussion

### 2.1 The reaction of $[Pt_6(CO)_6(SnCl_2)_2(SnCl_3)_4]^{4-}$ (**1**) with $HBf_4$ : Synthesis and characterization of $[Pt_{12}(CO)_{10}(SnCl)_2(SnCl_2)_4\{Cl_2Sn(\mu-OH)SnCl_2\}_2]^{2-}$ (**3**).

The title compound  $[Pt_{12}(CO)_{10}(SnCl)_2(SnCl_2)_4\{Cl_2Sn(\mu-OH)SnCl_2\}_2]^{2-}$  (**3**) was obtained by reacting  $[Pt_6(CO)_6(SnCl_2)_2(SnCl_3)_4]^{4-}$  (**1**) in  $CH_3CN$  with an excess of  $HBf_4 \cdot Et_2O$ , followed by removal of the solvent *in vacuo* and dissolving the residue in  $CH_2Cl_2$  (Scheme 1). The resulting solution displayed an unique  $\nu_{CO}$  carbonyl stretching band at  $2070\text{ cm}^{-1}$ .



**Scheme 1.** Syntheses of **3** and **4**.

Crystals of  $[PPh_4]_2[Pt_{12}(CO)_{10}(SnCl)_2(SnCl_2)_4\{Cl_2Sn(\mu-OH)SnCl_2\}_2]$  ( $[PPh_4]_2[**3**]$ ) suitable for X-ray analyses were obtained from slow diffusion of n-hexane on the  $CH_2Cl_2$  solution, confirming that the final

species formed was the dianion **3**. Crystals of **3** displayed  $\nu_{\text{CO}}$  at 2085(w), 2067(vs)  $\text{cm}^{-1}$  as solid in nujol mull, and at 2070(vs)  $\text{cm}^{-1}$  once dissolved in  $\text{CH}_2\text{Cl}_2$ , pointing out that the species was not altered during crystallization and/or dissolution of the crystals. The  $^1\text{H}$  NMR spectrum of  $[\text{PPh}_4]_2[\mathbf{3}]$  in  $\text{CD}_2\text{Cl}_2$  displayed the typical resonances of the  $[\text{PPh}_4]^+$  cation at  $\delta_{\text{H}}$  7.64–7.96 ppm (40H) and a broad resonance at  $\delta_{\text{H}}$  6.93 ppm (2H) attributable to the OH groups (Figure 1).

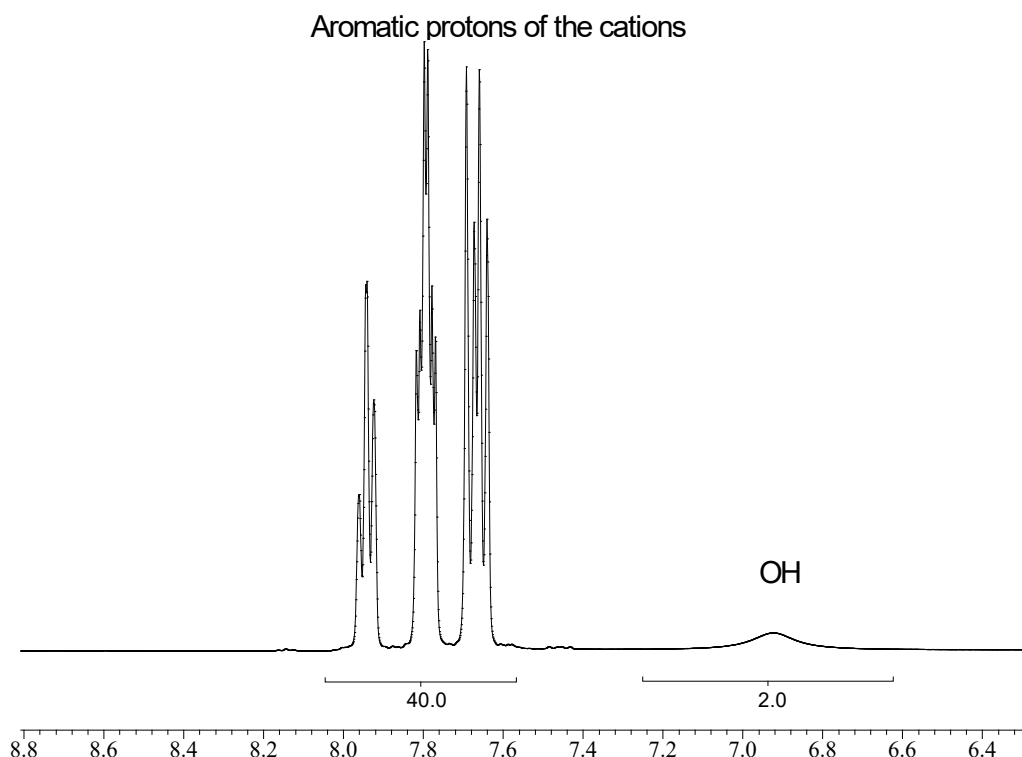


**Fig. 1.**  $^1\text{H}$  NMR spectrum recorded at 298 K in  $\text{CD}_2\text{Cl}_2$  of  $[\text{PPh}_4]_2[\mathbf{3}]$  with integrals.

A sample of  $\mathbf{3}\text{-}^{13}\text{CO}$  was prepared from the reaction of  $\mathbf{1}\text{-}^{13}\text{CO}$  with  $\text{HBF}_4\cdot\text{Et}_2\text{O}$ . Unfortunately, the  $^{13}\text{C}$  NMR spectra of  $\mathbf{3}\text{-}^{13}\text{CO}$  displayed only very broad resonances centred at  $\delta_{\text{C}}$  190 ppm at all temperatures studied (193–298 K), suggesting a very fast fluxional behaviour of the carbonyl ligands (Figure 2). The chemical shift observed for these very broad resonances was in agreement with the data previously reported for the parent cluster  $\mathbf{1}\text{-}^{13}\text{CO}$  [4]. For the latter it was possible to stop the exchange at 243 K, and two distinct resonances at  $\delta_{\text{C}}$  181.9 and 192.5 ppm appeared due to the presence of two different types of terminal CO ligands in  $\mathbf{1}\text{-}^{13}\text{CO}$  [4].

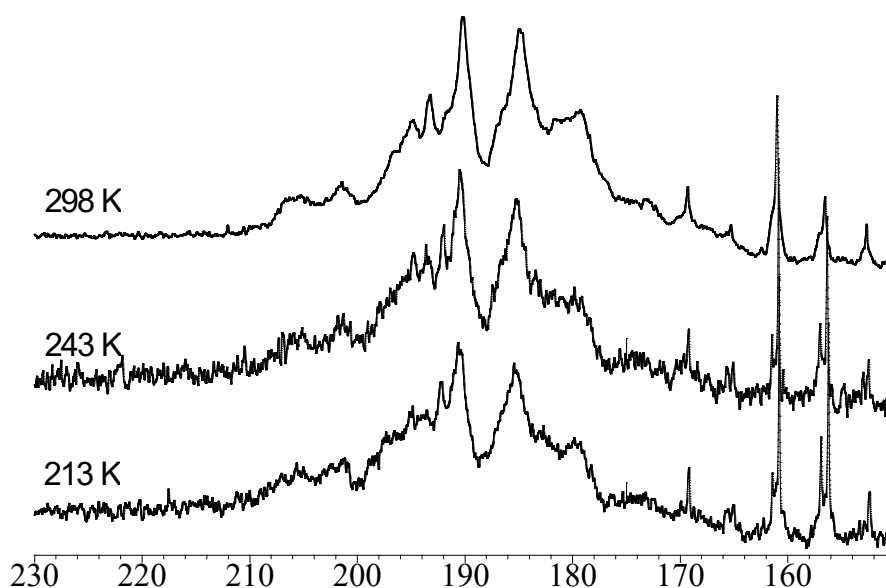


**Fig. 2.** VT  $^{13}\text{C}$  NMR spectra in  $\text{CD}_2\text{Cl}_2$  of  $\mathbf{3}\text{-}^{13}\text{CO}$ .

The molecular structure of **3** was determined as its  $[\text{PPh}_4]_2[\mathbf{3}]$  salt (Figure 3 and Table 1). The cluster anion is located on a 2-fold axis and the H-atom bonded to O(6) was initially located on the Fourier map and, then, refined by a riding model. An inter-molecular H-bond involving O(6)-H(6) and Cl(5)#1 [O(6)-H(6) 0.95 Å, H(6)⋯Cl(5)#1 2.14 Å, O(6)⋯Cl(5)#1 3.063(8) Å,  $\angle\text{O(6)H(6)Cl(5)\#1}$  164.9°; symmetry operation #1 –  $x+1/2, y-1/2, -z+1/2$ ] is present corroborating the location of H(6) (Figure 4) [23]. Because of the 2-fold symmetry, each cluster anion contains two O(6)-H(6) hydrogen-bond donors and two Cl(5) acceptor groups. This produces extended planes perpendicular to the crystallographic  $c$  axis of H-bonded cluster anions, with the  $[\text{PPh}_4]^+$  cations occupying the inter-layer positions (Figure S1 in the Supporting Information). This represents a rare case of a supramolecular arrangement of anionic metal carbonyl clusters *via* H-bonds [24].

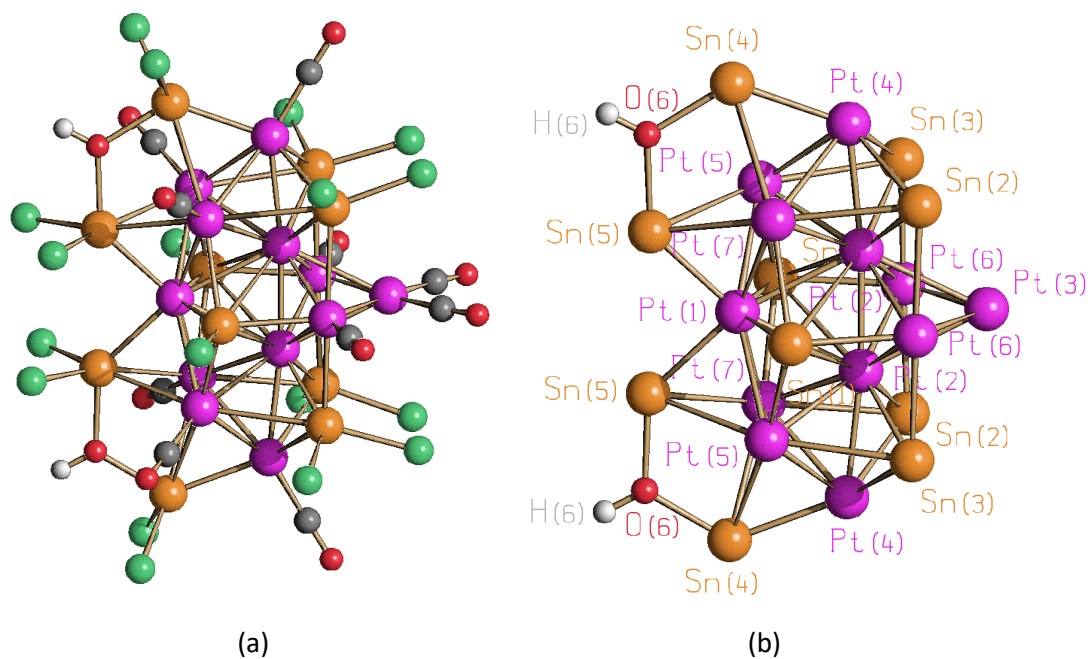


**Fig. 3.** (a) Molecular structure of  $[Pt_{12}(CO)_{10}(SnCl)_2(SnCl_2)_4\{Cl_2Sn(\mu-OH)SnCl_2\}_2]^{2-}$  (**3**) and (b) its  $Pt_{12}Sn_{10}$  metal core with labelling (purple, Pt; orange, Sn; green, Cl; red, O; grey, C).



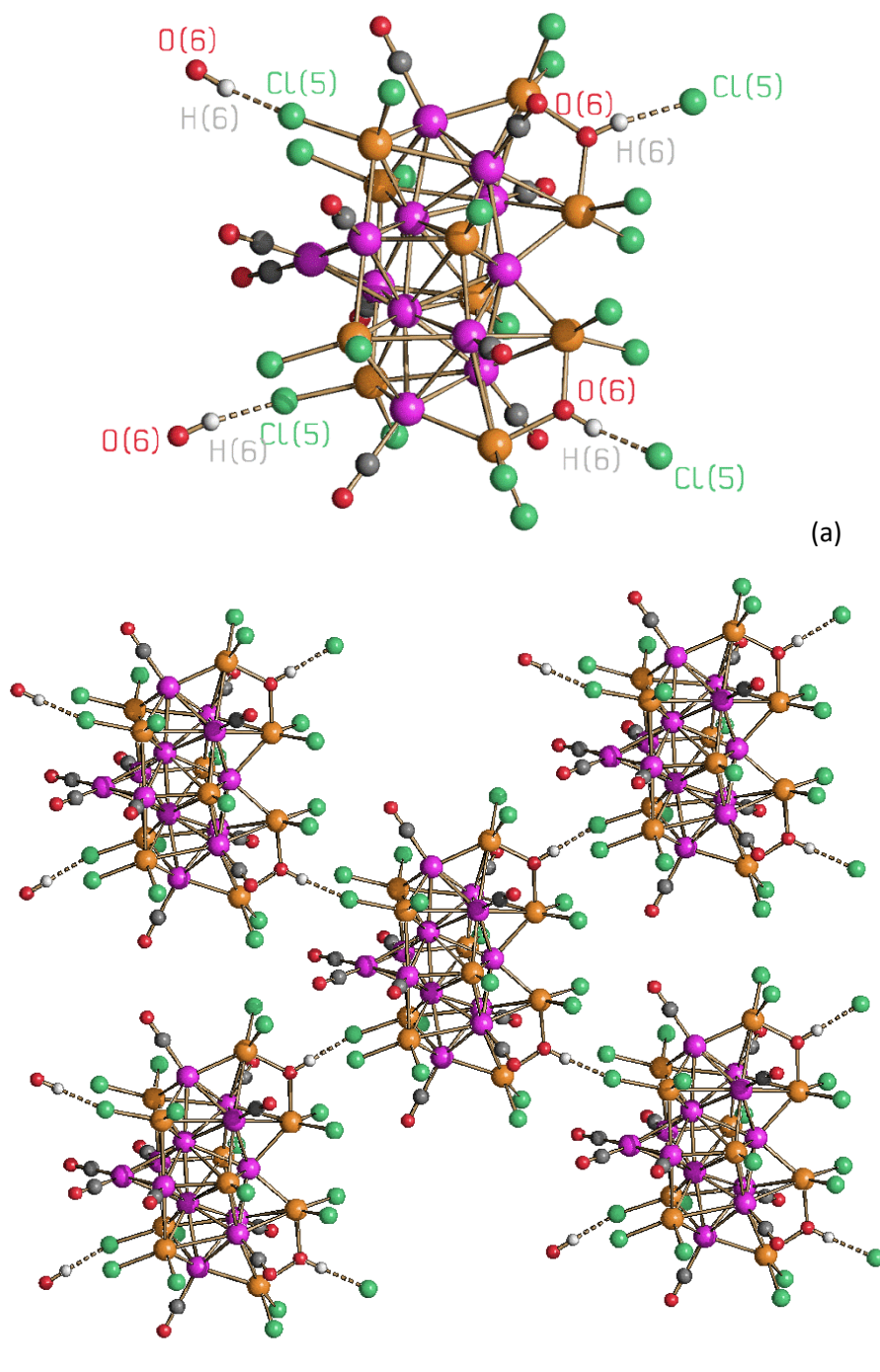


**Fig. 4.** H-bonds involving the  $[\text{Pt}_{12}(\text{CO})_{10}(\text{SnCl}_2)_2(\text{SnCl}_2)_4\{\text{Cl}_2\text{Sn}(\mu\text{-OH})\text{SnCl}_2\}_2]^{2-}$  (**3**) anion. (a) A single molecule is reported with its two OH-donors and Cl-acceptor groups with labelling. (b) Five molecules are represented (purple, Pt; orange, Sn; green, Cl; red, O; grey, C; white, H; H-bonds as dashed lines).

**Table 1**

Comparison of the most relevant bond lengths (Å) of  $[\text{Pt}_{12}(\text{CO})_{10}(\text{SnCl})_2(\text{SnCl}_2)_4\{\text{Cl}_2\text{Sn}(\mu\text{-OH})\text{SnCl}_2\}_2]^{2-}$  (**3**) and  $[\text{Pt}_7(\text{CO})_6(\text{SnBr}_2)_4\{\text{Br}_2\text{Sn}(\mu\text{-OH})\text{SnBr}_2\}\{\text{Br}_2\text{Sn}(\mu\text{-Br})\text{SnBr}_2\}]^{2-}$  (**4**).

	Pt-Pt	Pt-Sn	Sn-X
<b>3</b>	2.5837(7)-2.9883(6) Average 2.7970(19)	2.5854(8)-3.3505(7) Average 2.840(4)	2.331(3)-2.380(3) Average 2.359(9)
<b>4</b>	2.6947(5)-3.2450(5) Average 2.8434(12)	2.6256(9)-3.2991(9) Average 2.792(3)	2.4669(18)-2.789(3) Average 2.546(6)

Regarding the molecular anion (Figure 5), **3** consists of three  $\text{Pt}_5$  trigonal bipyramids (TBP) sharing three vertices and originating a common  $\text{Pt}_3$  triangle (in blue in Figure 5). The resulting  $\text{Pt}_{12}$  framework displays idealized  $C_{2v}$  and crystallographic  $C_2$  symmetry. Each of the two (symmetry related)  $\{\text{Cl}_2\text{Sn}(\mu\text{-OH})\text{SnCl}_2\}^-$  ligands is  $\eta^2\text{-}\mu_4$ -bonded to two adjacent triangular faces of a TBP, as previously found in  $[\text{Pt}_5(\text{CO})_5\{\text{Cl}_2\text{Sn}(\text{OR})\text{SnCl}_2\}_3]^{3-}$  ( $\text{R} = \text{H}, \text{Me}, \text{Et}, \text{}^i\text{Pr}$ ) [2]. The four  $\text{SnCl}_2$  stannylene ligands are  $\mu_4$ -bonded to open butterfly surfaces, whereas the two  $[\text{SnCl}]^+$  ligands are  $\mu_6$ -bonded to “triangular crown”  $\text{Pt}_6$  frames, where the central triangular unit is represented by the three Pt atoms shared by the three  $\text{Pt}_5$ TBPs [Pt(1), Pt(2), Pt(2)] and the wingtips are Pt(5), Pt(6) and Pt(7). The former three Pt atoms are not bonded to any CO, whereas the remaining nine Pt atoms are bonded to one terminal CO each, a part Pt(3) which is bonded to two terminal carbonyls.

**3** possesses 162 CVE (Cluster Valence Electron) [ $12 \times 10$  (12Pt) +  $10 \times 2$  (10CO) +  $2 \times 2$  ( $2[\text{SnCl}]^+$ ) +  $4 \times 2$  ( $4[\text{SnCl}_2]$ ) +  $2 \times 4$  ( $2\{\text{Cl}_2\text{Sn}(\mu\text{-OH})\text{SnCl}_2\}^-$ ) +  $2$  ( $2-$ )], as expected on the basis of Mingos's fusion formalism for a  $\text{M}_{12}$  cluster composed of three trigonal bipyramids sharing three vertices [ $72 \times 3$  (TBP) –  $18 \times 3$  (vertex) = 162 CVE] [25,26]. The same electron count is also obtained by describing this condensed cluster as the fusion of three TBP clusters and one triangle sharing three edges [ $72 \times 3$  (TBP) +  $48 \times 1$  (triangle) –  $34 \times 3$  (edges) = 162 CVE]. This electron count is based on the assumption that each Sn atom of the  $[\text{SnCl}]^+$ ,  $[\text{SnCl}_2]$  and  $[\text{Cl}_2\text{Sn}(\mu\text{-OH})\text{SnCl}_2]^-$  fragments acted as a two-electron donor (Scheme 2).

This item was downloaded from IRIS Università di Bologna (<https://cris.unibo.it/>)

**When citing, please refer to the published version.**

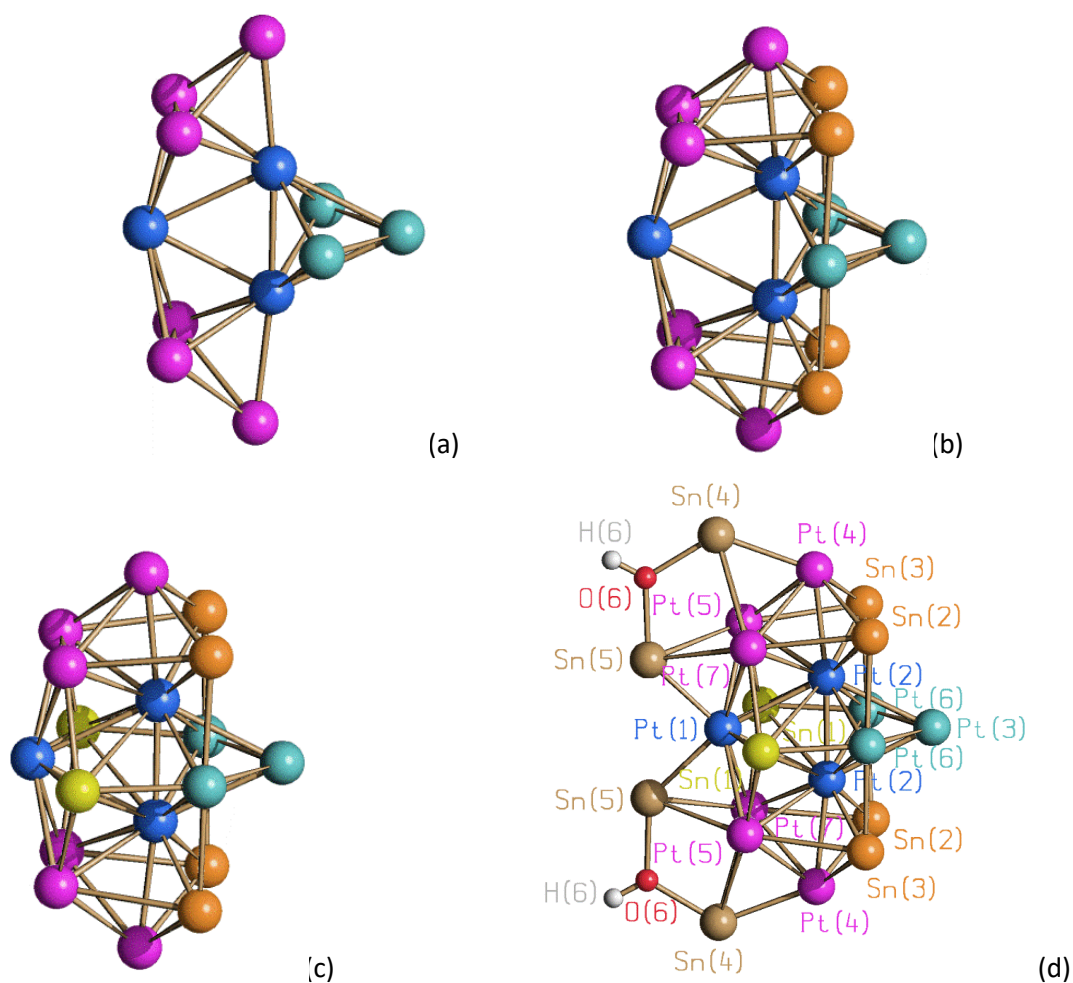
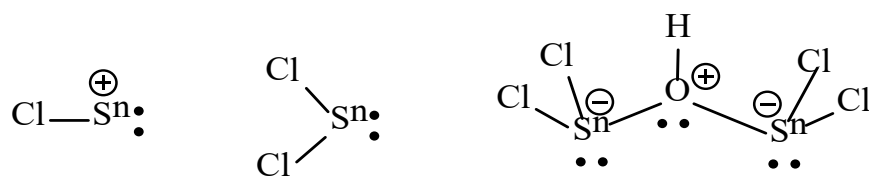


**Fig. 5.** (a) The  $\text{Pt}_{12}$  core of  $[\text{Pt}_{12}(\text{CO})_{10}(\text{SnCl})_2(\text{SnCl}_2)_4\{\text{Cl}_2\text{Sn}(\mu\text{-OH})\text{SnCl}_2\}_2]^{2-}$  (**3**) composed of three trigonal bipyramids (two related by  $C_2$  in purple, the third in cyan) sharing three vertices (in blue the common triangle). (b) The  $\text{Pt}_{12}\text{Sn}_4$  framework obtained by addition of four  $[\text{SnCl}_2]$  ligands to (a) (Sn in orange). (c) The  $\text{Pt}_{12}\text{Sn}_6$  framework resulting from the addition of two  $[\text{SnCl}]^+$  (yellow) ligands to (b). (d) The final  $\text{Pt}_{12}\text{Sn}_{10}$  framework including the two  $[\text{Cl}_2\text{Sn}(\text{OH})\text{SnCl}_2]^-$  bidentate ligands (tin in brown) with labelling.



**Scheme 2.** Lewis dot formulas of the  $[\text{SnCl}]^+$ ,  $[\text{SnCl}_2]$  and  $[\text{Cl}_2\text{Sn}(\mu\text{-OH})\text{SnCl}_2]^-$  fragments displaying the ability of each Sn-atom to act as a two-electron donor.

2.2 The reaction of  $[\text{Pt}_6(\text{CO})_6(\text{SnBr}_2)_2(\text{SnBr}_3)_4]^{4-}$  (**2**) with  $\text{HBF}_4$ : Synthesis and characterization of  $[\text{Pt}_7(\text{CO})_6(\text{SnBr}_2)_4\{\text{Br}_2\text{Sn}(\mu\text{-OH})\text{SnBr}_2\}\{\text{Br}_2\text{Sn}(\mu\text{-Br})\text{SnBr}_2\}]^{2-}$  (**4**).

The reaction of  $[\text{Pt}_6(\text{CO})_6(\text{SnBr}_2)_2(\text{SnBr}_3)_4]^{4-}$  (**2**) with an excess of  $\text{HBF}_4 \cdot \text{Et}_2\text{O}$  under the same conditions described in Section 2.1 afforded the new  $[\text{Pt}_7(\text{CO})_6(\text{SnBr}_2)_4\{\text{Br}_2\text{Sn}(\mu\text{-OH})\text{SnBr}_2\}\{\text{Br}_2\text{Sn}(\mu\text{-Br})\text{SnBr}_2\}]^{2-}$  (**4**) cluster dianion instead of a Br-congener of **3** (**3<sup>Br</sup>**). In order to shed light on this point, the structure of **3<sup>Br</sup>** was computationally optimized and showed to be comparable to that of **3** (*vide infra*). Thus, the different outcome of the reactions of  $[\text{Pt}_6(\text{CO})_6(\text{SnX}_2)_2(\text{SnX}_3)_4]^{4-}$  ( $\text{X} = \text{Cl}$ , **1**;  $\text{Br}$ , **2**), with  $\text{HBF}_4 \cdot \text{Et}_2\text{O}$  was not simply related to the instability of a purported **3<sup>Br</sup>**, but it arose from more complicated (and not yet clear) thermodynamic and kinetic effects. Indeed, **3** and **4** are supposed to be formed *via* complex mechanisms that, in the absence of any further experimental or theoretical support, could not be envisaged.

The  $\text{CH}_2\text{Cl}_2$  solution of **4** displayed an unique  $\nu_{\text{CO}}$  carbonyl stretching band at  $2064\text{ cm}^{-1}$ . Orange-red crystals of  $[\text{PPh}_4]_2[\text{Pt}_7(\text{CO})_6(\text{SnBr}_2)_4\{\text{Br}_2\text{Sn}(\mu\text{-OH})\text{SnBr}_2\}\{\text{Br}_2\text{Sn}(\mu\text{-Br})\text{SnBr}_2\}]$  containing the dianion **4** were obtained by slow diffusion of n-hexane on the  $\text{CH}_2\text{Cl}_2$  solution. The formation of these orange-red crystals was accompanied by minor amounts of a few yellow crystals, that revealed to be a mixture of  $[\text{PPh}_4][\text{Pt}(\text{CO})(\text{Br})(\text{SnBr}_3)_2]$  and  $[\text{PPh}_4]_2[\text{Pt}_2(\text{CO})_2(\text{Br})_4(\text{SnBr}_2)]$ . These were side-products of the synthesis of **4**, which were formed from the partial oxidation of the anionic cluster in the presence of an excess of strong acid.

The  $\text{Pt}_7$  core of the cluster **4** is composed of two  $\text{Pt}_4$  tetrahedra that share a common vertex located on a crystallographic inversion centre (Figure 6). The four  $\text{SnBr}_2$  stannylene ligands are  $\mu_4$ -bonded to the  $\text{Pt}_7$  core resulting in a bicapped centred pseudo-cubic  $\text{Pt}_7\text{Sn}_4$  framework. The  $\{\text{Br}_2\text{Sn}(\mu\text{-OH})\text{SnBr}_2\}^-$  and  $\{\text{Br}_2\text{Sn}(\mu\text{-Br})\text{SnBr}_2\}^-$  ligands are  $\eta^2$ - $\mu_3$ -bonded to two opposite (related by the inversion centre) triangular faces of the  $\text{Pt}_7$  core. The cluster contains a fully interstitial Pt atom. The remaining six Pt atoms are bonded to one terminal CO ligand each. The OH group of the  $\{\text{Br}_2\text{Sn}(\mu\text{-OH})\text{SnBr}_2\}^-$  ligand is involved in a weak  $\text{O-H}\cdots\pi$  interaction with one Ph ring of a  $[\text{PPh}_4]^+$  cation [ $\text{O-H}\cdots\text{C}_t$   $2.96\text{ \AA}$ ,  $< \text{O-H}\cdots\text{C}_t$   $153^\circ$ ;  $\text{C}_t$  centroid of the Ph ring] (Figure S2 in the Supporting Information) [27]. The  $^1\text{H}$  NMR spectrum of  $[\text{PPh}_4]_2[\text{4}]$  in  $\text{CD}_2\text{Cl}_2$  solution (Figure S3 in the Supporting Information) displays the typical resonances of the  $[\text{PPh}_4]^+$  cations at  $\delta_{\text{H}}$  7.64-7.96 ppm (40H) and a broad resonance at  $\delta_{\text{H}}$  3.14 ppm that integrated 1.4H. This resonance might be assigned to the OH group of **4** or to some adventitious water.

**4** possesses 98 CVE [ $7 \times 10$  (7Pt) +  $6 \times 2$  (6CO) +  $4 \times 2$  ( $4[\text{SnBr}_2]$ ) +  $2 \times 2$  ( $[\text{Br}_2\text{Sn}(\mu\text{-OH})\text{SnBr}_2]^-$ ) +  $2 \times 2$  ( $[\text{Br}_2\text{Sn}(\mu\text{-Br})\text{SnBr}_2]^-$ )], and is electron poor since 102 CVE ( $60 \times 2$  (Td) –  $18 \times 1$  (vertex) = 102 CVE) are expected for a  $\text{M}_7$  cluster composed of two tetrahedra sharing one vertex. A literature survey displays that

This item was downloaded from IRIS Università di Bologna (<https://cris.unibo.it/>)

**When citing, please refer to the published version.**

several heptanuclear clusters, whose structures are based on two vertex-sharing tetrahedra, have been structurally characterized and these showed 94-102 CVE [28-31].

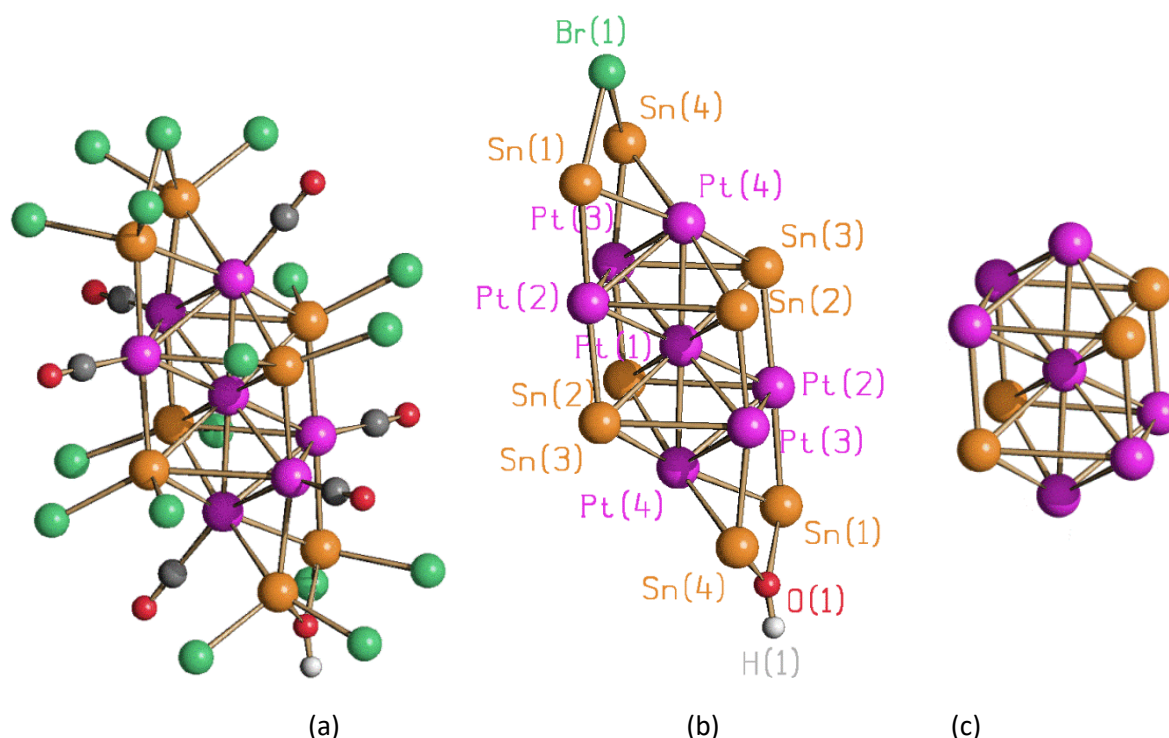


**Fig. 6.** (a) Molecular structure of  $[\text{Pt}_7(\text{CO})_6(\text{SnBr}_2)_4\{\text{Br}_2\text{Sn}(\mu\text{-OH})\text{SnBr}_2\}\{\text{Br}_2\text{Sn}(\mu\text{-Br})\text{SnBr}_2\}]^{2-}$  (**4**), (b) its  $\text{Pt}_7\text{Sn}_8$  metal core (the  $\mu\text{-OH}$  and  $\mu\text{-Br}$  groups are represented for sake of clarity) with labelling, and (c) its bicapped centred pseudo-cubic  $\text{Pt}_7\text{Sn}_4$  framework (purple, Pt; orange, Sn; green, Br; red, O; grey, C; white, H).

The crystals of the  $[\text{PPh}_4][\text{Pt}(\text{CO})(\text{Br})(\text{SnBr}_3)_2]$  and  $[\text{PPh}_4]_2[\text{Pt}_2(\text{CO})_2(\text{Br})_4(\text{SnBr}_2)]$  side products of the synthesis of **4** contain the new anionic complexes  $[\text{Pt}(\text{CO})(\text{Br})(\text{SnBr}_3)_2]^-$  (**5**) and  $[\text{Pt}_2(\text{CO})_2(\text{Br})_4(\text{SnBr}_2)]^{2-}$  (**6**) (Figure 7). **5** is a square-planar Pt(II) complex with two  $[\text{SnBr}_3]^-$  ligands in relative *trans*-position, one bromide and one carbonyl. Such CO-complex is unprecedented, whereas related square planar Pt-complexes containing two  $[\text{SnX}_3]^-$  and one  $\text{X}^-$  ligands have been previously reported [32]. **6** contains two square planar *cis*- $\text{PtBr}_2(\text{CO})$  moieties joined by a bridging  $\text{SnBr}_2$  group, as found in  $[\text{Pt}_2(\text{CO})_2(\text{I})_2(\text{PR}_3)_2(\text{SnCl}_2)]$  (R = cyclo-hexyl) and related species [7,8,33].

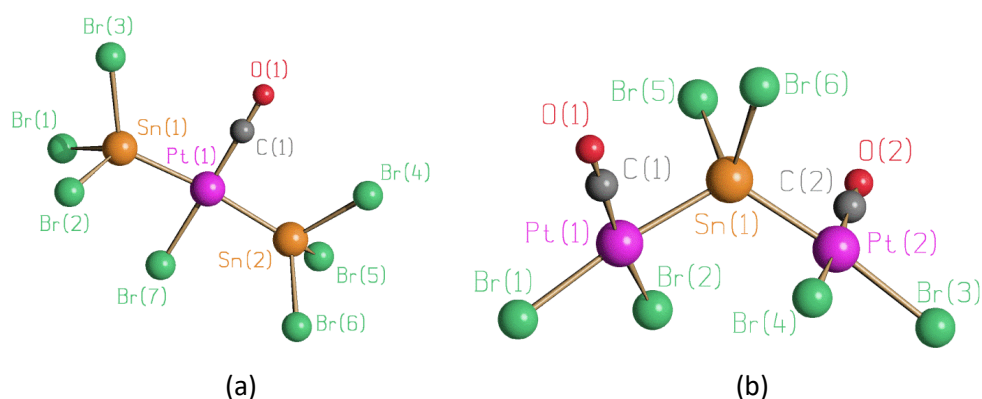


**Fig. 7** Molecular structures of (a)  $[\text{Pt}(\text{CO})(\text{Br})(\text{SnBr}_3)_2]^-$  (**5**) and (b)  $[\text{Pt}_2(\text{CO})_2(\text{Br})_4(\text{SnBr}_2)]^{2-}$  (**6**) with labelling (purple, Pt; orange, Sn; green, Br; red, O; grey, C).

### 2.3. Computational investigations

DFT calculations at  $\omega\text{B97X-v}$  level on the anion of compound **3**, using the geometry determined by X-ray diffraction, allowed the study of the metal-metal bonds by Atoms-In-Molecules (AIM) analysis. In the structure depicted in Figure 8 only the interactions characterized by (3,-1) bond critical points (b.c.p.) are shown. AIM calculations confirm the  $C_2$  symmetry of the molecule, only one set of b.c.p. is reported in Figure 8. Data concerning the metal-metal b.c.p. are summarized in Table 2. On considering the entire molecule, the number of bonds that Sn centres make with Pt is extremely variable: 1 for Sn(4), 3 for Sn(2), Sn(3) and Sn(5), and 4 for Sn(1), this last having only one coordinated chloride. The number and type of bonds formed by the Pt centres is also quite different: Pt(1) is bonded to 6 Pt and 4 Sn, Pt(2) to 7 Pt and 2 Sn, Pt(3) to 3 Pt and 0 Sn, Pt(4) to 2 Pt and 3 Sn, Pt(5) to 4 Pt and 2 Sn, Pt(6) to 3 Pt and 3 Sn, Pt(7) to 4 Pt and 2 Sn. Despite these differences, the Hirshfeld population analysis indicates that the partial charges among both Pt and Sn are quite similar (see Table 3), suggesting no change in the formal oxidation state. The only slightly positive charge value for Pt is obtained for Pt(3), the one not bonded to Sn centres. On the other hand, the most negative charge is obtained for Pt(2). The Pt charge range is however quite limited, about 0.12 a.u. The Sn Hirshfeld charges are around 0.26 a.u. with the exceptions of the OH-bonded Sn(4) and Sn(5), where the charge is more positive, about 0.34 a.u., in agreement with the higher deformation of Sn electron density caused by the bond with the electronegative oxygen atom. On attributing 2+ formal charge to the Sn centers, 1- formal charge to the chloro- and hydroxo-ligands and zero charge to the carbonyl ligands, the average Pt formal oxidation state is slightly lower than zero.



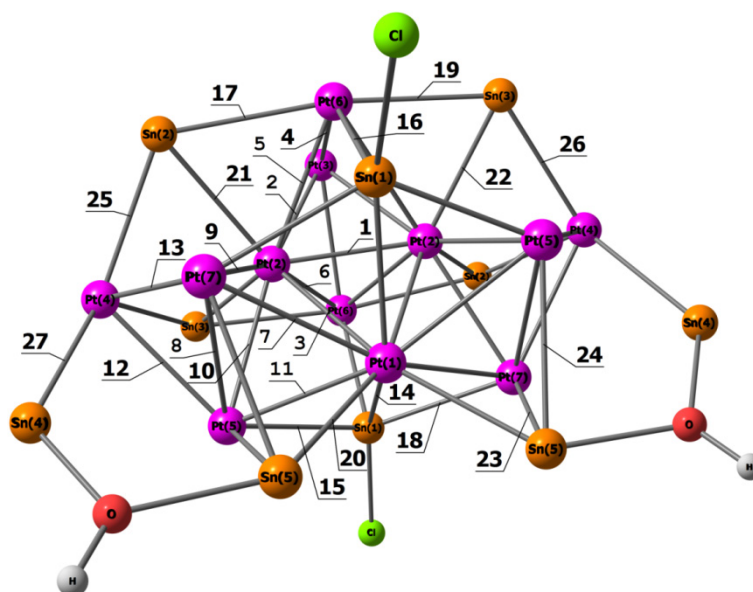


**Fig. 8.** Structure of the anion of compound **3** with bonds characterized by the presence of (3,-1) b.c.p. and their numbering. CO ligands and chlorides bonded to  $[\text{SnCl}_2]$  fragments are omitted for clarity. Colour map: purple, Pt; orange, Sn; green, Cl; red, O; white, H.

All the (3,-1) b.c.p. are characterized by negative values of electron densities ( $E$ ) and positive values for the Laplacian of electron density ( $\nabla^2\rho$ ), in agreement with Bianchi's definitions of M-M bonds [34]. On considering the density ( $\rho$ ) and the potential energy density ( $V$ ) values, the strongest Pt-Pt bond is that between the two Pt(2), while the weakest are those between Pt(5) and Pt(7). For what concerns the Pt-Sn interactions the strongest are between Pt(1) and Sn(5) and the weakest between Pt(5) and Sn(5). As observable in the Supporting Information (Figure S4) once defined the couple of attractors the potential energy density values are roughly related to the M-M' bond lengths, *i.e.* the most negative value corresponds to the shortest distance.

**Table 2**

Properties of the metal-metal (3,-1) b.c.p in the anion of compound **3** (electron density,  $\rho$ ; potential energy density,  $V$ ; energy density,  $E$ ; Laplacian of electron density,  $\nabla^2\rho$ ). All quantities in a.u.

b.c.p.	bond	$\rho$	$V$	$E$	$\nabla^2\rho$	b.c.p.	bond	$\rho$	$V$	$E$	$\nabla^2\rho$
1	Pt(2)-Pt(2)	0.076	-0.080	-0.023	0.137	14	Sn(1)-Pt(1)	0.050	-0.045	-0.013	0.079
2	Pt(2)-Pt(3)	0.044	-0.038	-0.092	0.077	15	Sn(1)-Pt(5)	0.063	-0.059	-0.020	0.077
3	Pt(1)-Pt(2)	0.045	-0.039	-0.010	0.080	16	Sn(1)-Pt(6)	0.062	-0.058	-0.019	0.078
4	Pt(3)-Pt(6)	0.058	-0.050	-0.016	0.076	17	Sn(2)-Pt(6)	0.055	-0.046	-0.016	0.059

This item was downloaded from IRIS Università di Bologna (<https://cris.unibo.it/>)

**When citing, please refer to the published version.**

5	Pt(2)-Pt(6)	0.057	-0.052	-0.015	0.087	18	Sn(1)-Pt(7)	0.064	-0.060	-0.020	0.080
6	Pt(2)-Pt(6)	0.058	-0.053	-0.015	0.089	19	Sn(3)-Pt(6)	0.055	-0.046	-0.016	0.059
7	Pt(1)-Pt(7)	0.045	-0.039	-0.010	0.075	20	Sn(5)-Pt(1)	0.072	-0.069	-0.024	0.080
8	Pt(5)-Pt(7)	0.041	-0.031	-0.009	0.053	21	Sn(2)-Pt(2)	0.060	-0.058	-0.017	0.095
9	Pt(2)-Pt(7)	0.061	-0.059	-0.017	0.101	22	Sn(3)-Pt(2)	0.062	-0.062	-0.018	0.101
10	Pt(2)-Pt(5)	0.061	-0.057	-0.016	0.097	23	Sn(5)-Pt(7)	0.042	-0.033	-0.009	0.059
11	Pt(1)-Pt(5)	0.049	-0.044	-0.011	0.086	24	Sn(5)-Pt(5)	0.038	-0.027	-0.007	0.052
12	Pt(4)-Pt(5)	0.052	-0.049	-0.013	0.094	25	Sn(2)-Pt(4)	0.056	-0.050	-0.016	0.070
13	Pt(4)-Pt(7)	0.050	-0.046	-0.012	0.089	26	Sn(3)-Pt(4)	0.057	-0.051	-0.017	0.071
						27	Sn(4)-Pt(4)	0.068	-0.066	-0.022	0.091

**Table 3**

Hirshfeld charges for Sn and Pt centres in the anion of compound **3** (a.u.).

M	charge	M	charge
Pt(1)	-0.038	Sn(1)	0.263
Pt(2)	-0.091	Sn(2)	0.264
Pt(3)	0.033	Sn(3)	0.262
Pt(4)	-0.007	Sn(4)	0.342
Pt(5)	-0.016	Sn(5)	0.349
Pt(6)	-0.004		
Pt(7)	-0.009		

Figure 9 shows the structure of compound **4** with the M-M bonds characterized by (3,-1) b.c.p. The main data concerning the b.c.p. are summarized in Table 4, while the Hirshfeld charges on the metal centres are collected in Table 5. As for cluster **3**, AIM data for Pt-Pt and Sn-Pt (3,-1) b.c.p. agree with the classification of M-M bonds [34]. Critical points are numbered accordingly to an inversion centre localized on Pt(1), despite the fact that the presence of two different bridging fragments,  $\mu$ -Br and  $\mu$ -OH, broke the symmetry. AIM data however indicate a quite symmetric electronic distribution in the cluster, in particular for what concerns the central core. Pt(1) is bonded to 6 Pt and 4 Sn and its coordination sphere could be best described, accordingly to the output of the SHAPE software [35], as a distorted HD-10 hexadecahedron (2:6:2). The inset of Figure 9 shows the superposition of the coordination sphere of Pt(1) with the hexadecahedron (2:6:2). Pt(2), Pt(3), Pt(5) and Pt(6) are bonded to 2 Pt and 2 Sn, and finally Pt(4) and Pt(7) are bonded to 3 Pt and 4 Sn. Every Sn centre is connected to two Pt. The strongest Pt-Pt bonds are, accordingly to the density and potential energy density values, those between Pt(1) and the Pt(2), Pt(5), Pt(4) and Pt(7) centres. On the other hand, the weakest Pt-Pt bonds are the Pt(2)-Pt(4) and Pt(5)-Pt(7) ones. For what concerns the Pt-Sn bonds, the highest  $\rho$  values are present at Sn(1)-Pt(2) and Sn(5)-Pt(5) b.c.p. As previously described for compound **3**, also for **4** the potential energy density values at b.c.p. are

*This item was downloaded from IRIS Università di Bologna (<https://cris.unibo.it/>)*

***When citing, please refer to the published version.***



approximately related to the Pt-Pt and Pt-Sn bond lengths (see Figure S5 in the Supporting Information). The Hirshfeld charge distribution is quite homogeneous among the Pt centres and the most negative charge is localized on the central Pt(1). The average Pt charge is strictly comparable with that of compound **3**, despite the fact that the formal oxidation state of the Pt centers in **4** is zero. As for compound **3**, the more positively charged Sn centres are those bonded to  $\mu$ -OH.

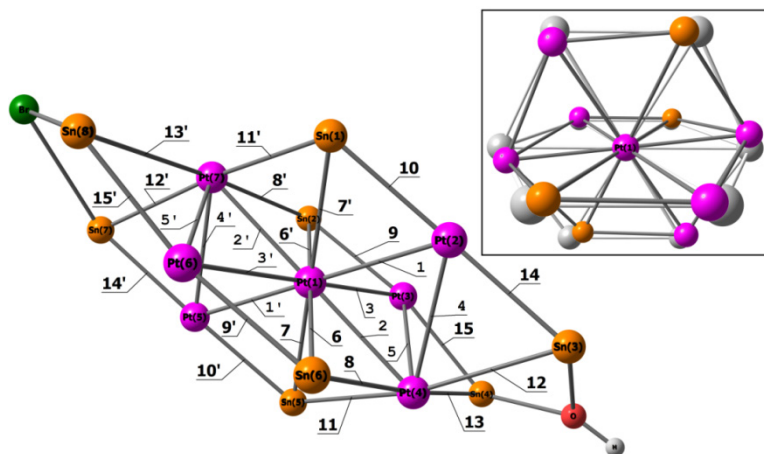


**Fig. 9.** Structure of the anion of compound **4** with bonds characterized by the presence of (3,-1) b.c.p. and their numbering. CO ligands and bromides bonded to  $[\text{SnBr}_2]$  fragments are omitted for clarity. Colour map: purple, Pt; orange, Sn; green, Br; red, O; white, H. Inset: superposition of the coordination sphere of Pt(1) with the corresponding hexadecahedron (2:6:2) in light grey tones.

**Table 4**

Properties of the metal-metal (3,-1) b.c.p in the anion of compound **4** (electron density,  $\rho$ ; potential energy density,  $V$ ; energy density,  $E$ ; Laplacian of electron density,  $\nabla^2\rho$ ). All quantities in a.u.

b.c.p.	bond	$\rho$	$V$	$E$	$\nabla^2\rho$	b.c.p.	bond	$\rho$	$V$	$E$	$\nabla^2\rho$
1	Pt(1)-Pt(2)	0.063	-0.059	-0.018	0.098	6	Sn(6)-Pt(1)	0.059	-0.057	-0.017	0.087
1'	Pt(1)-Pt(5)	0.063	-0.059	-0.018	0.098	6'	Sn(2)-Pt(1)	0.059	-0.057	-0.017	0.087
2	Pt(1)-Pt(4)	0.061	-0.058	-0.017	0.096	7	Sn(5)-Pt(1)	0.055	-0.050	-0.015	0.082
2'	Pt(1)-Pt(7)	0.061	-0.058	-0.017	0.097	7'	Sn(1)-Pt(1)	0.055	-0.050	-0.015	0.083
3	Pt(1)-Pt(3)	0.057	-0.051	-0.015	0.087	8	Sn(6)-Pt(4)	0.055	-0.046	-0.016	0.056
3'	Pt(1)-Pt(6)	0.057	-0.051	-0.015	0.087	8'	Sn(2)-Pt(7)	0.055	-0.046	-0.016	0.056
4	Pt(2)-Pt(4)	0.049	-0.041	-0.012	0.069	9	Sn(2)-Pt(3)	0.065	-0.057	-0.021	0.059
4'	Pt(5)-Pt(7)	0.049	-0.041	-0.012	0.069	9'	Sn(6)-Pt(6)	0.065	-0.057	-0.021	0.061
5	Pt(3)-Pt(4)	0.055	-0.047	-0.014	0.075	10	Sn(1)-Pt(2)	0.068	-0.061	-0.023	0.064
5'	Pt(6)-Pt(7)	0.055	-0.047	-0.014	0.075	10'	Sn(5)-Pt(5)	0.068	-0.061	-0.023	0.064
						11	Sn(5)-Pt(4)	0.059	-0.050	-0.018	0.058

This item was downloaded from IRIS Università di Bologna (<https://cris.unibo.it/>)

**When citing, please refer to the published version.**

11'	Sn(1)-Pt(7)	0.059	-0.051	-0.018	0.058
12	Sn(3)-Pt(4)	0.054	-0.044	-0.015	0.058
12'	Sn(7)-Pt(7)	0.054	-0.045	-0.015	0.059
13	Sn(4)-Pt(4)	0.052	-0.042	-0.014	0.054
13'	Sn(8)-Pt(7)	0.052	-0.042	-0.014	0.057
14	Sn(3)-Pt(2)	0.066	-0.061	-0.021	0.077
14'	Sn(7)-Pt(5)	0.065	-0.061	-0.021	0.078
15	Sn(4)-Pt(3)	0.065	-0.058	-0.020	0.070
15'	Sn(8)-Pt(6)	0.064	-0.058	-0.020	0.075

**Table 5**

Hirshfeld charges for Sn and Pt centres in the anion of compound **4** (a.u.).

M	charge	M	charge
Pt(1)	-0.099	Sn(1)	0.211
Pt(2)	-0.012	Sn(2)	0.218
Pt(3)	-0.009	Sn(3)	0.307
Pt(4)	-0.031	Sn(4)	0.313
Pt(5)	-0.012	Sn(5)	0.212
Pt(6)	-0.007	Sn(6)	0.217
Pt(7)	-0.031	Sn(7)	0.250
		Sn(8)	0.278

The Hirshfeld and AIM analyses have been extended for comparison to the electronic structures of the anions  $[\text{Pt}(\text{CO})(\text{Br})(\text{SnBr}_3)_2]^-$  (**5**) and  $[\text{Pt}_2(\text{CO})_2(\text{Br})_4(\text{SnBr}_2)]^{2-}$  (**6**), where Pt is coordinated to tin bromide moieties. Unlike **3** and **4**, the Pt centers have slightly positive charge, 0.084 a.u. in **5** and 0.096 a.u. in **6**. On the other hand, the Sn Hirshfeld charges of the  $[\text{SnBr}_2]$  fragments in **4** are comparable to that found for the bridging  $[\text{SnBr}_2]$  ligand in **6**, 0.216 a.u.

Despite the different formal Pt oxidation state, some of the Pt- $[\text{SnBr}_2]$  bonds in **4** have  $\rho$  and  $V$  values comparable with those computed for **5** and **6** (see Table 6), Sn(2)-Pt(3) and Sn(6)-Pt(6) in particular. The other Pt- $[\text{SnBr}_2]$  interactions in **4** are characterized by lower electron densities at b.c.p. The Pt-Sn bonds in **5** and **6** fall into the classification already described for the compounds **3** and **4** [34], but it is worth noting that  $\nabla^2\rho$  values are less positive, suggesting more electron shared interactions with respect to **3** and **4**.

**Table 6**

Average properties of the Pt-Sn (3,-1) b.c.p in the anions of compounds **5** and **6** (electron density,  $\rho$ ; potential energy density,  $V$ ; energy density,  $E$ ; Laplacian of electron density,  $\nabla^2\rho$ ). All quantities in a.u.

*This item was downloaded from IRIS Università di Bologna (<https://cris.unibo.it/>)*

***When citing, please refer to the published version.***

Compound	bond	$\rho$	V	E	$\nabla^2\rho$
5	Pt-Sn	0.069	-0.056	-0.023	0.042
6	Pt-Sn	0.075	-0.063	-0.027	0.040

The formation of cluster **4** instead of a bromo-compound analogous to **3** prompted us to carry out the DFT optimization of cluster **3** with chlorides replaced by bromides (**3<sup>Br</sup>**). The DFT optimized structure is closely comparable to that of **3**, as observable in Figure 10, where the metallic cores of the two species are superposed. The root-mean-square deviation between the two structures, once removed the halides, is only 0.120 Å. The energy values of the frontier orbitals are strictly comparable between **3** and **3<sup>Br</sup>** (**3**:  $E_{\text{HOMO}} = -4.271$  eV,  $E_{\text{LUMO}} = 0.893$  eV; **3<sup>Br</sup>**:  $E_{\text{HOMO}} = -4.219$  eV,  $E_{\text{LUMO}} = 0.745$  eV). The Hirshfeld charge distribution on Pt atoms in **3<sup>Br</sup>** is almost identical with respect to that of **3**. The lower electronegativity of bromine causes only the expected slight reduction of the positive charges on the Sn centres. No simple ground-state features of **3<sup>Br</sup>** are therefore able to explain the formation of compound **4** as final product.

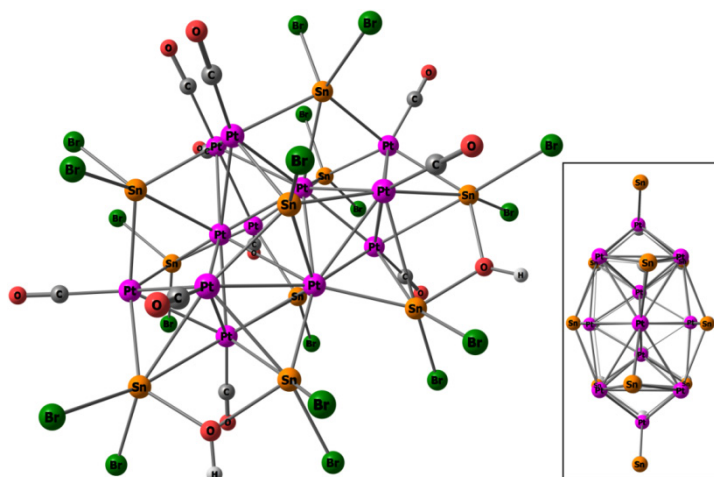


**Fig. 10.** DFT-optimized structure of the anion of **3<sup>Br</sup>**. Inset: superposition of the metallic core of **3<sup>Br</sup>** with that of **3**. Colour map: purple, Pt; orange, Sn; green, Br; red, O; grey, C; white, H. Compound **3** is depicted in light grey tones.

### 3. Conclusions

Two new Pt carbonyl clusters decorated by Sn(II) fragments were synthesised and structurally characterized. Their metal cores derived from the condensation of simple Pt polyhedra, that is three trigonal bipyramids in the case of **3** and two tetrahedra for **4**.

*This item was downloaded from IRIS Università di Bologna (<https://cris.unibo.it/>)*

**When citing, please refer to the published version.**

The formal oxidation state of Pt was  $-0.167$  and  $0$  for **3** and **4**, respectively. Such Pt cores were stabilised via the coordination of CO and Sn(II)-based ligands. DFT calculations corroborated these conclusions and showed that these molecular clusters contained strong Pt-Pt, Pt-CO, Pt-Sn, Sn-X and Sn-O bonds. As stated in the introduction, Sn acted somehow as a bridge between the low valent Pt-CO core and the external shell of  $X^-$  and  $OH^-$  ligands. This might be related to the ability of Sn to stabilise sub-nanometric Pt aggregates on the surface of metal oxide supports [36-38]. Indeed, such supports can be considered as ligands by providing their binding sites for metal atoms, clusters and nanoparticles [39]. As a general conclusion, molecular clusters are useful models for understanding at the atomic level the chemistry of nanometric and sub-nanometric metal aggregates [21,40-44]. More in specific, **3** and **4** could be used as precursors for the preparation of heterogeneous catalysts, as previously demonstrated for **1** [20]. The different compositions and structures of these clusters might lead to catalysts with different properties. Eventually, it has been also confirmed that strong acids can be employed for the structural rearrangement and growth of metal carbonyl clusters, leading to larger species [21,22].

## 4. Experimental Section

### 4.1 General procedures.

All reactions and sample manipulations were carried out using standard Schlenk techniques under nitrogen and in dried solvents. All the reagents were commercial products (Aldrich) of the highest purity available and used as received, except  $[PPh_4]_4[Pt_6(CO)_6(SnX_2)_2(SnX_3)_4]$  ( $X = Cl, Br$ ) which has been prepared according to the literature [3]. Analysis of Pt and Sn were performed by atomic absorption on a Pye-Unicam instrument. Analyses of C, H and N were obtained with a Thermo Quest Flash EA 1112NC instrument. IR spectra were recorded on a Perkin Elmer Spectrum One interferometer in  $CaF_2$  cells.  $^1H$  and  $^{13}C\{^1H\}$  NMR measurements were performed on a Varian Mercury Plus 400 MHz instrument. The proton and carbon chemical shifts were referenced to the non-deuterated aliquot of the solvent, whereas the phosphorous chemical shifts were referenced to external  $H_3PO_4$  (85% in  $D_2O$ ).  $^{13}CO$  enriched samples have been prepared starting from  $[PPh_4]_2[Pt_{12}(^{13}CO)_{24}]$  (ca. 40%  $^{13}CO$ ) [45]. Structure drawings have been performed with SCHAKAL99 [46].

### 4.2 Synthesis of $[PPh_4]_2[Pt_{12}(CO)_{10}(SnCl)_2(SnCl_2)_4\{Cl_2Sn(\mu-OH)SnCl_2\}_2]$ ( $[PPh_4]_2$ [**3**])

$HBf_4 \cdot Et_2O$  (500  $\mu$ l, 3.67 mmol) was added in small portions over a period of 2 h to a solution of  $[PPh_4]_4[Pt_6(CO)_6(SnCl_2)_2(SnCl_3)_4]$  (0.910 g, 0.282 mmol) in  $CH_3CN$  (30 mL). After the addition of the first 300  $\mu$ l of  $HBf_4 \cdot Et_2O$  the solution turned from green to brown and the unique  $\nu_{CO}$  band moved from 2038

This item was downloaded from IRIS Università di Bologna (<https://cris.unibo.it/>)

**When citing, please refer to the published version.**

to 2046 cm<sup>-1</sup>; this further moved to 2056 cm<sup>-1</sup> after the addition of other 200 µl of HBF<sub>4</sub>·Et<sub>2</sub>O. The solvent was, then, removed *in vacuo* and the residue dissolved in CH<sub>2</sub>Cl<sub>2</sub> (20 mL), where it displayed a single ν<sub>CO</sub> band at 2066 cm<sup>-1</sup>. Crystals of [PPh<sub>4</sub>]<sub>2</sub>[Pt<sub>12</sub>(CO)<sub>10</sub>(SnCl)<sub>2</sub>(SnCl<sub>2</sub>)<sub>4</sub>{Cl<sub>2</sub>Sn(μ-OH)SnCl<sub>2</sub>}<sub>2</sub>] suitable for X-ray analyses were obtained from slow diffusion of n-hexane (40 mL) on the CH<sub>2</sub>Cl<sub>2</sub> solution (yield 0.386 g, 53 % based on Pt). Yield is given as the amount of crystals effectively isolated. Some of **3** remained in the CH<sub>2</sub>Cl<sub>2</sub>/n-hexane after diffusion. Moreover, some side products not soluble in CH<sub>2</sub>Cl<sub>2</sub> remained during the work-up. Among them, it was possible to identify the starting material **1**, that was soluble in CH<sub>3</sub>CN and identified by IR spectroscopy.

C<sub>58</sub>H<sub>42</sub>Cl<sub>18</sub>O<sub>12</sub>P<sub>2</sub>Pt<sub>12</sub>Sn<sub>10</sub> (5158.94): calcd. C 13.49, H 0.82, Sn 23.24, Pt 45.34; found: C 13.81, H 1.12, Sn 23.04, Pt 45.62. IR (nujol, 293 K) ν<sub>CO</sub>: 2067(s) cm<sup>-1</sup>. IR (CH<sub>2</sub>Cl<sub>2</sub>, 293 K) ν<sub>CO</sub>: 2069(s) cm<sup>-1</sup>.

Samples of [PPh<sub>4</sub>]<sub>2</sub>[Pt<sub>12</sub>(<sup>13</sup>CO)<sub>10</sub>(SnCl)<sub>2</sub>(SnCl<sub>2</sub>)<sub>4</sub>{Cl<sub>2</sub>Sn(μ-OH)SnCl<sub>2</sub>}<sub>2</sub>] can be prepared starting from [PPh<sub>4</sub>]<sub>4</sub>[Pt<sub>6</sub>(<sup>12</sup>CO)<sub>8</sub>(SnCl)<sub>2</sub>(SnCl<sub>3</sub>)<sub>4</sub>] and following the same procedure as above. [PPh<sub>4</sub>]<sub>2</sub>[Pt<sub>12</sub>(<sup>13</sup>CO)<sub>10</sub>(SnCl)<sub>2</sub>(SnCl<sub>2</sub>)<sub>4</sub>{Cl<sub>2</sub>Sn(μ-OH)SnCl<sub>2</sub>}<sub>2</sub>] displays ν(<sup>13</sup>CO) in CH<sub>2</sub>Cl<sub>2</sub> at 2019(s) cm<sup>-1</sup>.

<sup>1</sup>H NMR (CD<sub>2</sub>Cl<sub>2</sub>, 298 K) δ (ppm): 7.64-7.96 (m, 40H, Ph), 6.93 (br, 2H, OH).

<sup>13</sup>C{<sup>1</sup>H} NMR (CD<sub>2</sub>Cl<sub>2</sub>, 298 K) δ (ppm) <sup>13</sup>CO enriched sample (only the CO region is given): 185.0 (br), 190.2 (br). <sup>13</sup>C{<sup>1</sup>H} NMR (CD<sub>2</sub>Cl<sub>2</sub>, 243 K) δ (ppm): 185.2 (br), 190.5 (br). <sup>13</sup>C{<sup>1</sup>H} NMR (CD<sub>2</sub>Cl<sub>2</sub>, 213 K) δ (ppm): 185.5 (br), 190.7 (br).

#### 4.3 Synthesis of [PPh<sub>4</sub>]<sub>2</sub>[Pt<sub>7</sub>(CO)<sub>6</sub>(SnBr<sub>2</sub>)<sub>4</sub>{Br<sub>2</sub>Sn(μ-OH)SnBr<sub>2</sub>}{Br<sub>2</sub>Sn(μ-Br)SnBr<sub>2</sub>}] ([PPh<sub>4</sub>]<sub>2</sub>[**4**])

HBF<sub>4</sub>·Et<sub>2</sub>O (500 µl, 3.67 mmol) was added in small portions over a period of 2 h to a solution of [PPh<sub>4</sub>]<sub>4</sub>[Pt<sub>6</sub>(CO)<sub>6</sub>(SnCl<sub>2</sub>)<sub>2</sub>(SnCl<sub>3</sub>)<sub>4</sub>] (1.04 g, 0.282 mmol) in CH<sub>3</sub>CN (30 mL). The solvent was, then, removed *in vacuo* and the residue dissolved in CH<sub>2</sub>Cl<sub>2</sub> (20 mL). Orange-red crystals of [PPh<sub>4</sub>]<sub>2</sub>[Pt<sub>7</sub>(CO)<sub>6</sub>(SnBr<sub>2</sub>)<sub>4</sub>{Br<sub>2</sub>Sn(μ-OH)SnBr<sub>2</sub>}{Br<sub>2</sub>Sn(μ-Br)SnBr<sub>2</sub>}] suitable for X-ray analyses were obtained from slow diffusion of n-hexane (40 mL) on the CH<sub>2</sub>Cl<sub>2</sub> solution (yield 0.515 g, 47% based on Pt). The formation of these orange-red crystals was accompanied by a few yellow crystals of [PPh<sub>4</sub>][Pt(CO)(Br)(SnBr<sub>3</sub>)<sub>2</sub>] ([PPh<sub>4</sub>][**5**]) and [PPh<sub>4</sub>]<sub>2</sub>[Pt<sub>2</sub>(CO)<sub>2</sub>(Br)<sub>4</sub>(SnBr<sub>2</sub>)<sub>2</sub>] ([PPh<sub>4</sub>]<sub>2</sub>[**6**]). Crystals of [PPh<sub>4</sub>][**5**] and [PPh<sub>4</sub>]<sub>2</sub>[**6**] were mechanically separated from [PPh<sub>4</sub>]<sub>2</sub>[**4**] and their structures determined by means of single crystal X-ray diffraction. Since only a few crystals of [PPh<sub>4</sub>][**5**] and [PPh<sub>4</sub>]<sub>2</sub>[**6**] were obtained, yields were not registered.

[PPh<sub>4</sub>]<sub>2</sub>[Pt<sub>7</sub>(CO)<sub>6</sub>(SnBr<sub>2</sub>)<sub>4</sub>{Br<sub>2</sub>Sn(μ-OH)SnBr<sub>2</sub>}{Br<sub>2</sub>Sn(μ-Br)SnBr<sub>2</sub>}] C<sub>54</sub>H<sub>41</sub>Br<sub>17</sub>O<sub>7</sub>P<sub>2</sub>Pt<sub>7</sub>Sn<sub>8</sub> (4537.43): calcd. C 14.30, H 0.91, Sn 21.18, Pt 30.13; found: C 14.58, H 1.14, Sn 20.94, Pt 29.95. IR (nujol, 293 K) ν<sub>CO</sub>: 2060(s) cm<sup>-1</sup>. IR (CH<sub>2</sub>Cl<sub>2</sub>, 293 K) ν<sub>CO</sub>: 2064(s) cm<sup>-1</sup>.

<sup>1</sup>H NMR (CD<sub>2</sub>Cl<sub>2</sub>, 298 K) δ (ppm): 7.64-7.96 (m, 40H, Ph), 3.14 (br, 1H, OH).

This item was downloaded from IRIS Università di Bologna (<https://cris.unibo.it/>)

**When citing, please refer to the published version.**

[PPh<sub>4</sub>][Pt(CO)(Br)(SnBr<sub>3</sub>)<sub>2</sub>]. IR (nujol, 293 K)  $\nu(\text{CO})$ : 2088(s) cm<sup>-1</sup>.

#### 4.4 X-ray Crystallographic Study.

Crystal data and collection details for [PPh<sub>4</sub>]<sub>2</sub>[Pt<sub>12</sub>(CO)<sub>10</sub>(SnCl)<sub>2</sub>(SnCl<sub>2</sub>)<sub>4</sub>{Cl<sub>2</sub>Sn( $\mu$ -OH)SnCl<sub>2</sub>}]<sub>2</sub> ([PPh<sub>4</sub>]<sub>2</sub>[**3**]), [PPh<sub>4</sub>]<sub>2</sub>[Pt<sub>7</sub>(CO)<sub>6</sub>(SnBr<sub>2</sub>)<sub>4</sub>{Br<sub>2</sub>Sn( $\mu$ -OH)SnBr<sub>2</sub>}{Br<sub>2</sub>Sn( $\mu$ -Br)SnBr<sub>2</sub>}] ([PPh<sub>4</sub>]<sub>2</sub>[**4**]), [PPh<sub>4</sub>][Pt(CO)(Br)(SnBr<sub>3</sub>)<sub>2</sub>] ([PPh<sub>4</sub>][**5**]), and [PPh<sub>4</sub>]<sub>2</sub>[Pt<sub>2</sub>(CO)<sub>2</sub>(Br)<sub>4</sub>(SnBr<sub>2</sub>)] ([PPh<sub>4</sub>]<sub>2</sub>[**6**]), were reported in Table 6. The diffraction experiments were carried out on a Bruker APEX II diffractometer equipped with a CCD detector ([PPh<sub>4</sub>]<sub>2</sub>[**3**]) or a PHOTON100 detector ([PPh<sub>4</sub>]<sub>2</sub>[**4**], [PPh<sub>4</sub>][**5**] and [PPh<sub>4</sub>]<sub>2</sub>[**6**]) using Mo-K $\alpha$  radiation. Data were corrected for Lorentz polarization and absorption effects (empirical absorption correction SADABS) [47]. Structures were solved by direct methods and refined by full-matrix least-squares based on all data using  $F^2$  [48]. Hydrogen atoms were fixed at calculated positions and refined by a riding model. All non-hydrogen atoms were refined with anisotropic displacement parameters, unless otherwise stated.

**[PPh<sub>4</sub>]<sub>2</sub>[3]:** The asymmetric unit of the unit cell contained half of a cluster anion (located on 2) and one [PPh<sub>4</sub>]<sup>+</sup> cation (on a general position). The O-bonded H-atom was initially located in the Fourier Map and, then, refined by a riding model. Its position was confirmed by the presence of a O-H...Cl inter-molecular H-bond, involving O(6)-H(6) and Cl(5). Some alerts of level B were present in the checkcif. These were due to high values for the residual electron density. These maxima are located close to the Pt atoms, in positions which were not realistic for any atom, and they were series termination errors which are common with heavy atoms, especially in the case of high nuclearity clusters.

**[PPh<sub>4</sub>]<sub>2</sub>[4]:** The asymmetric unit of the unit cell contained half of a cluster anion (located on an inversion centre) and one [PPh<sub>4</sub>]<sup>+</sup> cation (on a general position). The atom bridging Sn(1) and Sn(4) was originally assigned to Br(1), resulting in an unsatisfactory refinement. The refinement was considerably improved assuming a disorder model and assigning this electron density to Br(1) and O(1)H(1) in a 1:1 ratio. As a result, the final model contained one {Br<sub>2</sub>Sn( $\mu$ -OH)SnBr<sub>2</sub>}<sup>-</sup> and one {Br<sub>2</sub>Sn( $\mu$ -Br)SnBr<sub>2</sub>}<sup>-</sup> ligand. The O-bonded H-atom was initially located in the Fourier Map and, then, refined by a riding model. Br(1) and O(1) were constrained to have the same anisotropic displacement parameters (EADP line in SHELXL). In order to confirm the nature of the above mentioned Br(1)/O(1)H(1) disorder, two independent crystals were collected. The cif files of both structures were deposited for sake of completeness. These two independent data sets recorded on different crystals confirmed the model that contained Br(1) and O(1)H(1) in a 1:1 ratio. Moreover, some alerts of level B were present in the checkcif. These were due to high values for the residual electron density. These maxima were located close to the Pt and Br atoms, in positions which were

This item was downloaded from IRIS Università di Bologna (<https://cris.unibo.it/>)

**When citing, please refer to the published version.**

not realistic for any atom, and they were series termination errors which are common with heavy atoms, especially in the case of high nuclearity clusters.

**[PPh<sub>4</sub>][5]:** The asymmetric unit of the unit cell contained one anion and one [PPh<sub>4</sub>]<sup>+</sup> cation all located on general positions. The C-atoms were restrained to have similar thermal parameters (SIMU line in SHELX, s.u. 0.01).

**[PPh<sub>4</sub>]<sub>2</sub>[6]:** The asymmetric unit of the unit cell contained one anion and one [PPh<sub>4</sub>]<sup>+</sup> cation all located on general positions.

**Table 6**

Crystal data and experimental details for [PPh<sub>4</sub>]<sub>2</sub>[3], [PPh<sub>4</sub>]<sub>2</sub>[4], [PPh<sub>4</sub>][5] and [PPh<sub>4</sub>]<sub>2</sub>[6].

	[PPh <sub>4</sub> ] <sub>2</sub> [3]	[PPh <sub>4</sub> ] <sub>2</sub> [4]
Formula	C <sub>58</sub> H <sub>42</sub> Cl <sub>18</sub> O <sub>12</sub> P <sub>2</sub> Pt <sub>12</sub> Sn <sub>10</sub>	C <sub>54</sub> H <sub>41</sub> Br <sub>17</sub> O <sub>7</sub> P <sub>2</sub> Pt <sub>7</sub> Sn <sub>8</sub>
<i>F</i> <sub>w</sub>	5158.94	4537.43
T, K	100(2)	100(2)
λ, Å	0.71073	0.71073
Crystal system	Monoclinic	Triclinic
Space Group	<i>C</i> 2/ <i>c</i>	<i>P</i> $\bar{1}$
<i>a</i> , Å	17.2741(5)	12.3993(13)
<i>b</i> , Å	20.8585(5)	13.8560(15)
<i>c</i> , Å	27.3924(8)	14.3072(15)
α, °	90	67.521(2)
β, °	95.259(2)	75.474(2)
γ, °	90	76.359(2)
Cell Volume, Å <sup>3</sup>	9828.3(5)	2171.6(4)
<i>Z</i>	4	1
<i>D</i> <sub>c</sub> , g cm <sup>-3</sup>	3.487	3.470
μ, mm <sup>-1</sup>	20.057	21.375
<i>F</i> (000)	9032	1992
Crystal size, mm	0.19×0.16×0.12	0.16×0.13×0.11
θ limits, °	1.534–27.000	1.610–26.000
Index ranges	-22 ≤ <i>h</i> ≤ 22 -26 ≤ <i>k</i> ≤ 26 -34 ≤ <i>l</i> ≤ 34	-15 ≤ <i>h</i> ≤ 15 -17 ≤ <i>k</i> ≤ 17 -17 ≤ <i>l</i> ≤ 17

This item was downloaded from IRIS Università di Bologna (<https://cris.unibo.it/>)

**When citing, please refer to the published version.**

Reflections collected	80522	26793
Independent reflections	10727 [ $R_{\text{int}} = 0.0963$ ]	8505 [ $R_{\text{int}} = 0.0485$ ]
Completeness to $\theta$ max	99.9%	99.8%
Data / restraints / parameters	10727 / 0 / 506	8505 / 6 / 391
Goodness on fit on $F^2$	1.036	1.089
$R_1$ ( $I > 2\sigma(I)$ )	0.0398	0.0401
$wR_2$ (all data)	0.1173	0.0839
Largest diff. peak and hole, $e \text{ \AA}^{-3}$	3.153 / -2.691	3.245 / -2.607

	[PPh <sub>4</sub> ][5]	[PPh <sub>4</sub> ] <sub>2</sub> [6]
Formula	C <sub>25</sub> H <sub>20</sub> Br <sub>7</sub> OPPtSn <sub>2</sub>	C <sub>50</sub> H <sub>40</sub> Br <sub>6</sub> O <sub>2</sub> P <sub>2</sub> Pt <sub>2</sub> Sn
$F_w$	1359.22	1723.09
T, K	100(2)	100(2)
$\lambda$ , Å	0.71073	0.71073
Crystal system	Triclinic	Monoclinic
Space Group	$P\bar{1}$	$P2_1/c$
a, Å	11.7995(6)	22.1246(16)
b, Å	12.4409(6)	13.9666(10)
c, Å	13.5990(7)	18.0304(14)
$\alpha$ , °	64.707(2)	90
$\beta$ , °	71.374(2)	110.363(2)
$\gamma$ , °	71.958(2)	90
Cell Volume, Å <sup>3</sup>	1675.04(15)	5223.3(7)
Z	2	4
$D_c$ , g cm <sup>-3</sup>	2.695	2.191
$\mu$ , mm <sup>-1</sup>	14.061	10.506
F(000)	1232	3208
Crystal size, mm	0.22×0.15×0.12	0.16×0.15×0.10
$\theta$ limits, °	1.849–26.997	1.758–26.000
Index ranges	-15 ≤ h ≤ 15 -15 ≤ k ≤ 15 -17 ≤ l ≤ 17	-27 ≤ h ≤ 27 -17 ≤ k ≤ 17 -22 ≤ l ≤ 22
Reflections collected	23334	63258
Independent reflections	7284 [ $R_{\text{int}} = 0.0655$ ]	10261 [ $R_{\text{int}} = 0.0909$ ]

This item was downloaded from IRIS Università di Bologna (<https://cris.unibo.it/>)

**When citing, please refer to the published version.**



Completeness to $\theta$ max	99.9%	100.0%
Data / restraints / parameters	7284 / 150 / 334	10261 / 12 / 568
Goodness on fit on $F^2$	1.074	1.058
$R_1$ ( $I > 2\sigma(I)$ )	0.0417	0.0430
$wR_2$ (all data)	0.0997	0.1070
Largest diff. peak and hole, $e \text{ \AA}^{-3}$	1.625 / -1.941	2.295 / -2.302

#### 4.5 Computational details.

The electronic structures of the anions of compounds **3** and **4** were optimized using the range-separated hybrid DFT functional  $\omega$ B97X-V, including non-local correlation by the VV10 functional [49]. Input Cartesian coordinates were obtained from X-ray diffraction data. The basis set used was the Ahlrichs' def2 split-valence, with polarization and diffusion functions and relativistic ECPs for Sn and Pt [50]. Geometry optimization of the **3**<sup>Br</sup> anion was carried out using the PBEh-3c method, which is a reparametrized version of PBE0 (with 42 % HF exchange) that uses a split-valence double-zeta basis set (def2-mSVP) and adds three corrections that consider dispersion, basis set superposition and other basis set incompleteness effects [51]. The geometries of **5** and **6** were optimized with the  $\omega$ B97X functional and the def2-SVPD basis set. Single point calculations on **3**<sup>Br</sup>, **5** and **6** were then performed at the previously described  $\omega$ B97X-V/def2-SVPD level. The "restricted" approach was used in all the cases. Calculations were performed with the ORCA 4.0.1.2 software [52]. The output, converted in .molden format, was used for AIM and Hirshfeld analyses, performed with the software Multiwfn, version 3.5 [53]. Cartesian coordinates of the DFT-optimized **3**<sup>Br</sup>, **5** and **6** anion are collected in a separated .xyz file.

#### Appendix A. Supplementary material

Cartesian coordinates of the DFT-optimized **3**<sup>Br</sup>, **5** and **6** anion as a .xyz file.

CCDC 1957040-1957044 contain the supplementary crystallographic data for this paper. These data can be obtained free of charge from the Cambridge Crystallographic Data Centre.

#### References

- [1] E. Brivio, A. Ceriotti, L. Garlaschelli, M. Manassero, M. Sansoni, J. Chem. Soc., Chem. Commun. (1995) 2055-2056.
- [2] A. Ceriotti, M. Daghetta, S. El Afeey, A. Ienco, G. Longoni, G. Manca, C. Mealli, S. Zacchini, S. Zarra, Inorg. Chem. 50 (2011) 12553-12561.

This item was downloaded from IRIS Università di Bologna (<https://cris.unibo.it/>)

**When citing, please refer to the published version.**

- [3] M. Bortoluzzi, A. Ceriotti, I. Ciabatti, R. Della Pergola, C. Femoni, M. C. Iapalucci, A. Storione, S. Zacchini, Dalton Trans. 45 (2016) 5001-5013.
- [4] M. Bortoluzzi, A. Ceriotti, C. Cesari, I. Ciabatti, R. Della Pergola, C. Femoni, M. C. Iapalucci, A. Storione, S. Zacchini, Eur. J. Inorg. Chem. (2016) 3939-3949.
- [5] (a) S. St. John, S. Ravindren, Z. Nan, K. Gunasekera, P. Boolchand, A. P. Angelopoulos, Appl. Surf. Sci. 448 (2018) 362-368; (b) S. St. John, N. Hu, D. W. Schaefer, A. P. Angelopoulos, J. Phys. Chem. C 117 (2013) 7924-7933.
- [6] M. S. Holt, W. L. Wilson, J. H. Nelson, Chem. Rev. 89 (1989) 11-49.
- [7] (a) T. Zöllner, C. Dietz, F. Winter, R. Pöttgen, S. I. Gorelsky, A. Hoffmann, S. Herres-Pawlis, K. Jurkschat, Chem. -Eur. J. 24 (2018) 5551-5561; (b) A. Albinati, R. Naegeli, K. H. A. O. Starewski, P. S. Pregosin, H. Rügger, Inorg. Chim. Acta 76 (1983) L231-L232.
- [8] (a) M. F. Lappert, R. S. Rowe, Coord. Chem. Rev. 100 (1990) 267-292; (b) M. Wagner, V. Deáky, C. Dietz, J. Martincová, B. Mahieu, R. Jambor, S. Herres-Pawlis, K. Jurkschat, Chem. Eur. J. 19 (2013) 6695-6708.
- [9] D. Das, S. S. Mohapatra, S. Roy, Chem. Soc. Rev. 44 (2015) 3666-3690.
- [10] (a) R. D. Adams, D. A. Blom, B. Captain, R. Raja, J. M. Thomas, E. Trufan, Langmuir 24 (2008) 9223-9226; (b) J. M. Thomas, R. D. Adams, E. M. Boswell, B. Captain, H. Grönbeck, R. Raja, Faraday Discuss. 138 (2008) 301-315.
- [11] (a) A. B. Hungria, R. Raja, R. D. Adams, B. Captain, J. M. Thomas, P. A. Midgley, V. Golvenko, B. F. G. Johnson, Angew. Chem. Int. Ed. 45 (2006) 4782-4785; (b) R. D. Adams, E. M. Boswell, B. Captain, A. B. Hungria, P. A. Midgley, R. Raja, J. M. Thomas, Angew. Chem. Int. Ed. 46 (2007) 8182-8185.
- [12] (a) R. D. Cortright, J. A. Dumestic, J. Catal. 148 (1994) 771-778; (b) R. D. Cortright, J. A. Dumestic, Appl. Catal. A 129 (1995) 101-115; (c) J. L. Margitfalvi, A. Tompos, I. Kolosova, J. Valyon, J. Catal. 174 (1998) 246-249.
- [13] (a) H. Rong, Z. Niu, Y. Zhao, H. Cheng, Z. Li, L. Ma, J. Li, S. Wei, Y. Li, Chem. Eur. J. 21 (2015) 12034-12041; (b) P. Gallezot, D. Richard, Catal. Rev. 40 (1998) 81-126; (c) C. Carnevillier, F. Epron, P. Marecot, Appl. Catal. A 275 (2004) 25-33.
- [14] (a) R. D. Cramer, E. L. Jenner, R. V. Lindsey, U. G. Stolberg, J. Am. Chem. Soc. 85 (1963) 1691-1692; (b) H. A. Tayim, J. C. Bailar, J. Am. Chem. Soc. 89 (1967) 4330-4338; (c) J. F. Knifton, J. Am. Oil Chem. Soc. 55 (1978) 496-500.

This item was downloaded from IRIS Università di Bologna (<https://cris.unibo.it/>)

**When citing, please refer to the published version.**

- [15] (a) L. Deng, H. Miura, T. Shishido, Z. Wang, S. Hosokawa, K. Teramura, T. Tanaka, J. Catal. 365 (2018) 277-291; (b) P. A. Zharova, A. V. Chistyakov, S. S. Shapovalov, A. A. Pasynskii, M. V. Tsodikov, Energy 172 (2019) 18-25; (c) J. Zhou, Y. Zhao, J. Zhang, Y. Wang, O. Y. Gutiérrez, S. Wang, Z. Li, P. Jin, S. Wang, X. Ma, J. A. Lercher, Chem. Commun. 54 (2018) 8818-8821.
- [16] (a) W. Du, G. Yang, E. Wong, N. A. Deskins, A. I. Frenkel, D. Su, X. Teng, J. Am. Chem. Soc. 136 (2014) 10862-10865; (b) C. Lamy, E. M. Belgsir, J. M. Léger, J. Appl. Electrochem. 31 (2001) 799-809; (c) W. Zhou, Z. Zhou, S. Song, W. Li, G. Sun, P. Tsiakaras, Q. Xin, Appl. Catal. B 46 (2003) 273-285.
- [17] (a) M. Li, A. Kowal, K. Sasaki, N. Marinkovic, D. Su, E. Korach, P. Liu, R. R. Adzic, Electrochim. Acta 55 (2010) 4331-4338; (b) W. Du, Q. Wang, C. A. LaScala, L. Zhang, D. Su, A. I. Frenkel, V. K. Mathur, X. Teng, J. Mater. Chem. 21 (2011) 8887-8892; (c) M. Li, D. A. Cullen, K. Sasaki, N. S. Marinkovic, K. More, R. R. Adzic, J. Am. Chem. Soc. 135 (2013) 132-141.
- [18] R. Tarozaitė, L. T. Tamašiūnaitė and V. Jasulaitienė, J. Solid. State Electrochem. 13 (2009) 721-731.
- [19] (a) J.-Y. Chen, S.-C. Lim, C.-H. Kuo, H.-Y. Tuan, J. Colloid. Interf. Sci. 545 (2019) 54-62; (b) H. C. Su, N. V. Myung, Electroanal. 31 (2019) 437-447.
- [20] D. Bonincontro, A. Lolli, A. Storione, A. Gasparotto, B. Berti, S. Zacchini, N. Dimitratos, S. Albonetti, Appl. Catal. A 588 (2019) 117279.
- [21] S. Zacchini, Eur. J. Inorg. Chem. (2011) 4125-4145.
- [22] (a) E. Cattabriga, I. Ciabatti, C. Femoni, M. C. Iapalucci, G. Longoni, S. Zacchini, Inorg. Chim. Acta 470 (2018) 238-249; (b) E. Cattabriga, I. Ciabatti, C. Femoni, T. Funaioli, M. C. Iapalucci, S. Zacchini, Inorg. Chem. 55 (2016) 6068-6079.
- [23] (a) G. R. Desiraju, Acc. Chem. Res. 35 (2002) 565-573; (b) G. R. Desiraju, Chem. Commun. (2005) 2995-3001.
- [24] (a) S. Aime, M. R. Chierotti, R. Gobetto, A. Russo, M. J. Stchedroff, Inorg. Chim. Acta 351 (2003) 251-255; (b) C. Femoni, M. C. Iapalucci, G. Longoni, S. Zacchini, E. Zazzaroni, Dalton Trans. (2007) 6644-2651.

- [25] (a) D. M. P. Mingos, D. J. Wales, Introduction to Cluster Chemistry, Prentice Hall, Englewood Cliffs, 1990; (b) D. G. Evans, D. M. P. Mingos, J. Organomet. Chem. 240 (1982) 321-327; (c) D. M. P. Mingos, T. Slee, L. Zhenyang, Chem. Rev. 90 (1990) 383-402.
- [26] (a) J.-F. Halet, D. G. Evans, D. M. P. Mingos, J. Am. Chem. Soc. 110 (1988) 87-90; (b) K. Wade, Adv. Inorg. Chem. Radiochem. 18 (1976) 1-66.
- [27] (a) M. Oki, H. Iwamura, J. Am. Chem. Soc. 89 (1967) 576-579; (b) D. Schollmeyer, O. V. Shishkin, T. Rühl, M. O. Vysotsky, Cryst. Eng. Commun. 10 (2008) 715-723.
- [28] (a) Y. Yamamoto, H. Yamazaki, T. Sakurai, J. Am. Chem. Soc. 104 (1982) 2329-2330; (b) R. D. Adams, M. Chen, Organometallics 31 (2012) 6457-6465.
- [29] (a) Y. Li, W.-T. Wong, Eur. J. Inorg. Chem. (2003) 2651-2662; (b) A. Albinati, K.-H. Dahmen, A. Togni, L. M. Venanzi, Angew. Chem. Int. Ed. 24 (1985) 766-767; (c) W.-T. Wong, Organometallics 18 (1999) 3474-3481.
- [30] (a) R. D. Adams, G. Chen, D. A. Katahira, J. T. Tanner, W. Wu, Inorg. Chem. 29 (1990) 3270-3272; (b) R. D. Adams, M. P. Pompeo, W. Wu, Inorg. Chem. 30 (1991) 2425-2432.
- [31] (a) J. W.-S. Hui, W.-T. Wong, J. Chem. Soc., Dalton Trans. (1997) 1515-1520; (b) N. de Silva, J. W. Laufenberg, L. F. Dahl, Chem. Commun. (2006), 4437-4439.
- [32] (a) N. W. Alcock, J. H. Nelson, J. Chem Soc., Dalton Trans. (1982) 2415-2418; (b) J. H. Nelson, W. L. Wilson, L. W. Cary, N. W. Alcock, H. J. Clase, G. S. Jas, L. Ramsey-Tassin, J. W. Kenney, Inorg. Chem. 35 (1996) 883-892.
- [33] Z. Béni, R. Ros, A. Tassan, R. Scopelliti, R. Roulet, Dalton Trans. (2005) 315-325.
- [34] (a) R. Bianchi, G. Gervasio, D. Marabello, Inorg. Chem. 39 (2000) 2360-2366; (b) C. Lepetit, P. Fau, K. Fajerwerg, M. L. Kahn, B. Silvi, Coord. Chem. Rev. 345 (2017) 150-181.
- [35] M. Llunell, D. Casanova, J. Cirera, P. Alemany, S. Alvarez. *SHAPE*, v2.1, Universitat de Barcelona and The Hebrew University of Jerusalem, Barcelona and Jerusalem (2013).
- [36] (a) N. Kamiuchi, T. Matsui, R. Kikuchi, K. Eguchi, J. Phys. Chem. C 111 (2007) 16470-16476; (b) N. Kamiuchi, K. Taguchi, T. Matsui, R. Kikuchi, K. Eguchi, Appl. Catal. B 89(2009) 65-72.
- [37] H. Xiong, S. Lin, J. Goetze, P. Pletcher, H. Guo, L. Kovarik, K. Artyushkova, B. M. Weckhuysen, A. K. Datye, Angew. Chem. Int. Ed. 56 (2017) 8986-8991.
- [38] B. Berti, C. Femoni, M. C. Iapalucci, S. Ruggieri, S. Zacchini, Eur. J. Inorg. Chem. (2018) 3285-3296.

This item was downloaded from IRIS Università di Bologna (<https://cris.unibo.it/>)

**When citing, please refer to the published version.**

- [39] P. Liu, R. Qin, G. Fu, N. Zheng, J. Am. Chem. Soc. 139 (2017) 2122-2131.
- [40] I. Ciabatti, C. Femoni, M. C. Iapalucci, G. Longoni, S. Zacchini, J. Cluster Sci. 25 (2014) 115-146.
- [41] L. M. Martínez-Prieto, B. Chaudret, Acc. Chem. Res. 51 (2018) 376-384.
- [42] R. Jin, C. Zeng, M. Zhou, Y. Chen, Chem. Rev. 116 (2016) 10346-10413.
- [43] I. Chakraborty, T. Pradeep, Chem. Rev. 117 (2017) 8208-8271.
- [44] B. Berti, I. Ciabatti, C. Femoni, M. C. Iapalucci, S. Zacchini, ACS Omega 3 (2018) 13239-13250.
- [45] C. Brown, B. T. Heaton, A. D. C. Towl, P. Chini, A. Fumagalli, G. Longoni, J. Organomet. Chem. 181 (1979) 233-254.
- [46] E. Keller, SCHAKAL99, University of Freiburg, Germany, 1999.
- [47] G. M. Sheldrick, SADABS-2008/1 - Bruker AXS Area Detector Scaling and Absorption Correction, Bruker AXS, Madison, Wisconsin, USA, 2008.
- [48] G. M. Sheldrick, Acta Cryst. C71 (2015) 3-8.
- [49] N. Mardirossian, M. Head-Gordon, Phys. Chem. Chem. Phys. 16 (2014) 9904-9924.
- [50] (a) F. Weigend, R. Ahlrichs, Phys. Chem. Chem. Phys. 7 (2005) 3297-3305; (b) D. Andrae, U. Häußermann, M. Dolg, H. Stoll, H. Preuß, Theor. Chim. Acta 77 (1990) 123-141.
- [51] S. Grimme, J. G. Brandenburg, C. Bannwarth, A. Hansen, J. Chem. Phys. 143 (2015) 054107.
- [52] (a) F. Neese, WIREs Comput. Mol. Sci. 2 (2012) 73-78; (b) F. Neese, WIREs Comput. Mol. Sci. 8 (2018) e1327.
- [53] T. Lu, F. Chen, J. Comput. Chem. 33 (2012) 580-592.